SKI Report 2008:11

Research

Discrete-Feature Modelling of Groundwater Flow and Solute Transport for SR-Can Review

External review contribution in support of SKI's and SSI's review of SR-Can

Joel Geier

March 2008

ISSN 1104-1374
ISRN SKI-R-08/11-SE

SKI Report 2008:11

Research

Discrete-Feature Modelling of Groundwater Flow and Solute Transport for SR-Can Review

External review contribution in support of SKI's and SSI's review of SR-Can

Joel Geier

Clearwater Hardrock Consulting
Corvallis, Oregon, USA

March 2008

Foreword

The work presented in this report is part of the Swedish Nuclear Power Inspectorate's (SKI) and the Swedish Radiation Protection Authority's (SSI) SR-Can review project.

The Swedish Nuclear Fuel and Waste Management Co (SKB) plans to submit a license application for the construction of a repository for spent nuclear fuel in Sweden 2010. In support of this application SKB will present a safety report, SR-Site, on the repository's long-term safety and radiological consequences. As a preparation for SR-Site, SKB published the preliminary safety assessment SR-Can in November 2006. The purposes were to document a first evaluation of long-term safety for the two candidate sites at Forsmark and Laxemar and to provide feedback to SKB's future programme of work.

An important objective of the authorities' review of SR-Can is to provide guidance to SKB on the complete safety reporting for the license application. The authorities have engaged external experts for independent modelling, analysis and review, with the aim to provide a range of expert opinions related to the sufficiency and appropriateness of various aspects of SR-Can. The conclusions and judgments in this report are those of the authors and may not necessarily coincide with those of SKI and SSI. The authorities own review will be published separately (SKI Report 2008:23, SSI Report 2008:04 E).

This report presents results of discrete feature modelling of groundwater flow and solute transport on a regional scale at SKB's candidate sites Laxemar and Forsmark.

Bo Strömberg (project leader SKI) Björn Dverstorp (project leader SSI)

Förord

Denna rapport är en underlagsrapport till Statens kärnkraftinspektions (SKI) och Statens strålskyddsinstituts (SSI) gemensamma granskning av Svensk Kärnbränslehantering AB:s (SKB) säkerhetsredovisning SR-Can.

SKB planerar att lämna in en ansökan om uppförande av ett slutförvar för använt kärnbränsle i Sverige under 2010. Som underlag till ansökan kommer SKB presentera en säkerhetsrapport, SR-Site, som redovisar slutförvarets långsiktiga säkerhet och radiologiska konsekvenser. Som en förberedelse inför SR-Site publicerade SKB den preliminära säkerhetsanalysen SR-Can i november 2006. Syftena med SR-Can är bl.a. att redovisa en första bedömning av den långsiktiga säkerheten för ett KBS-3-förvar vid SKB:s två kandidatplatser Laxemar och Forsmark och att ge återkoppling till SKB:s fortsatta arbete.

Myndigheternas granskning av SR-Can syftar till att ge SKB vägledning om förväntningarna på säkerhetsredovisningen inför den planerade tillståndsansökan. Myndigheterna har i sin granskning tagit hjälp av externa experter för oberoende modellering, analys och granskning. Slutsatserna i denna rapport är författarnas egna och överensstämmer inte nödvändigtvis med SKI:s eller SSI:s ställningstaganden. Myndigheternas egen granskning publiceras i en annan rapport (SKI Rapport 2008:19; SSI Rapport 2008:04).

Denna rapport redovisar modellering av grundvattenflöde och transport med diskreta nätverk på en regional skala inom SKB:s platsundersökningsområden Laxemar och Forsmark.

Bo Strömberg (projektledare SKI)   Björn Dverstorp (projektledare SSI)

Abstract

Discrete-feature models were developed to represent the main classes of water-conducting features at the Laxemar and Forsmark candidate sites for a high-level radioactive waste repository. The models encompass features on scales ranging from individual fractures 2 m or larger in radius around deposition holes, or spalled zones around deposition holes and tunnels, to deformation zones on the scale of kilometres. Equivalent discontinuum features are used to represent the aggregate properties of fractures outside of the vicinity of deposition holes where an explicit representation is used.

Deposition hole locations within the repository layout are conditioned to each stochastic realization of the discrete-fracture population, using a full-perimeter-intersection criterion to identify discriminating fractures that pose a seismic risk, and a simulated pilot-hole criterion to exclude deposition-hole locations with excessive flows. The utilization factors of $\varepsilon = 0.70$ obtained here for the full repository at Forsmark and $\varepsilon = 0.53$ for the full repository at Laxemar are significantly lower than the corresponding values $\varepsilon = 0.93$ and $\varepsilon = 0.88$ for the most nearly comparable case presented in Table 9-6 of the SR-Can Main Report (SKB, 2006b). Further investigation is needed to discern whether this discrepancy is primarily due to possible nonconservative assumptions in SKB's analytical modelling approach, or due to artefacts of the simulation approach using finite domains, which could lead to overly conservative values in the present study.

Flows through the discrete-feature model variants are calculated by finite-element simulation. Distributions of flows to deposition holes are presented for the Laxemar base case and for an initial suite of variants for Forsmark. Results for Forsmark indicate that the distribution of flow to deposition holes is robust with respect to the set of variants considered, and that a given single realization of the discrete-fracture network (DFN) submodel produces representative results. The variants completed thus far do not include alternative conceptual models for the DFN submodel, or variants with respect to its key properties, such as the assumed correlation of size to transmissivity.

The flow distribution to deposition holes is not strongly sensitive to the hydrologic properties of the large-scale deformation zones or the time-dependent boundary conditions

in a temperate setting. The main controls appear to be the DFN submodel, the excavation-damaged zone (EDZ) around tunnels, and spalled zones in the deposition-hole walls (if present).

Advective-dispersive particle-tracking results are presented for a suite of Forsmark model variants. A continuous EDZ intersecting all deposition holes and extending along all repository tunnels is included in all of these variants presented here. This is a significant feature for flow and transport, due to the apparent sparseness of the fracture population in the repository volume at Forsmark.

For the Forsmark model variants considered here, the safety-critical lower portion of the distribution of transport resistance F_r is not strongly sensitive to most of the variants that have been modelled. Spalling around deposition holes produces a slight reduction in the lowest values of F_r below about 2×10^3 yr/m, but apparently yields an increase in F_r for the remainder of the distribution. This result is likely sensitive to the assumptions regarding hydraulic properties of the spalled zones, which have been arbitrarily specified for lack of relevant data. Further investigation of the sensitivity of the F_r distribution to assumptions regarding these parameters is warranted.

The lower end of the F_r distribution also shows some sensitivity to stochastic realizations of the DFN submodel. This indicates that further exploration of uncertainties in the DFN submodel, including major conceptual uncertainties (clustering or hierarchical structure) is needed.

Table of contents

1 Introduction

This discrete-feature groundwater flow and solute transport modelling project was conducted to support a joint review by the Swedish Nuclear Power Inspectorate (SKI) and the Swedish Radiation Protection Institute (SSI), of the SR-Can preliminary safety assessment which was conducted by the Swedish Nuclear Fuel and Waste Management Company (SKB). According to the SR-Can Main Report (SKB, 2006b) the purposes of this preliminary safety assessment are:

1. To make a first assessment of the safety of potential KBS-3 repositories at Forsmark and Laxemar to dispose of canisters as specified in the application for the encapsulation plant.

2. To provide feedback to design development, to SKB's RD&D programme, to further site investigations and future safety assessment projects.

3. To foster a dialogue with the authorities that oversee SKB's activities regarding interpretation of applicable regulations, as a preparation for the SR-Site project.

In contrast with past safety assessment exercises which were to some extent generic, the SR-Can is based directly on site-specific data and interpretive models that have been developed in SKB's ongoing site investigations at the Forsmark and Laxemar sites. As such, this also represents an opportunity for the Swedish authorities to review SKB's methodology for utilizing site-specific data and site-specific conceptual models in safety assessment, prior to a license application.

1.1 Scope and objectives

The primary aim of this modelling project was to produce independent calculations of groundwater flowrates to deposition holes at the Forsmark and Laxemar sites, to support calculations of the risk of canister failure in a KBS-3 repository at these sites. A secondary aim was to produce estimates of radionuclide transport and retention properties for path from a hypothetical leaking canister to the biosphere, which could be used for calculations of dose and risk resulting from failure of the engineered barriers in the repository.

The models in this study are discrete-feature implementations of SKB's Site Descriptive Model (SDM) 1.2, for the Laxemar and Forsmark sites respectively. Post-closure, saturated conditions are assumed unless otherwise noted. Alternative interpretations of the model components, such as large-scale deformation zones (DZs) or the near-field discrete-fracture network (DFN), and alternative boundary conditions are treated as variations.

The models include site-specific representation of the repository layout according to SKB's D1 designs for the two sites. Backfill, buffer, and excavation-damage zone (EDZ) permeabilities for the base case are represented as equivalent discrete-features according to design specifications. Deposition holes are placed consistent with SKB's criteria for avoiding discriminating fractures. Deviations from the design properties due to effects such as spalling or shear displacements are considered as variations.

1.2 Organization of work and structure of report

The work undertaken in this project is based on the discrete-feature modelling concept. Models are constructed based on the geological and hydrogeological description of the sites and engineering designs. Hydraulic heads and flows through the network of water-conducting features are calculated by the finite-element method, and are used in turn to simulate migration of non-reacting solute by a particle-tracking method, in order to estimate the properties of pathways by which radionuclides could be released to the biosphere. Variants of the base-case model are used to explore the consequences of key aspects of uncertainty in the site descriptions. Stochastic simulation is used to evaluate portions of the model that can only be characterized in statistical terms, since many water-conducting features within the model volume cannot be characterized deterministically.

Chapter 2 describes the methodology by which discrete features are derived to represent water-conducting features around the hypothetical repositories, including both natural features and features that result from the disturbance of excavation, and then assembled to produce a discrete-feature network model for numerical simulation of flow and transport.

Chapter 3 describes how site-specific data and repository designs are adapted to produce discrete-feature models for the two sites, and how variants are defined to evaluate key aspects of uncertainty.

Results of the calculations are presented in Chapter 4. These include utilization factors for deposition tunnels based on the emplacement criteria that have been set forth by the implementers, flow distributions to the deposition holes for the different variants, and calculated properties of discharge paths as well as locations of discharge to the biosphere. Chapters 5 and 6 present a discussion of these results and the conclusions.

2 Methodology

2.1 Discrete-feature conceptual model

The discrete-feature conceptual model represents deformation zones, individual fractures, and other water-conducting features around a repository as discrete conductors surrounded by a rock matrix which, in the present study, is treated as impermeable. This approximation is reasonable given the very low permeability of granitic rock excluding macroscopic fracturing.

A feature is represented as a planar or piecewise-planar surface, described at each point $\vec{\xi}$ on its surface by effective 2-D parameters of transmissivity $T(\vec{\xi})$, storativity $S(\vec{\xi})$, and transport aperture $b(\vec{\xi})$. In the present study, these parameters are taken to be uniform over all segments of a given feature.

The boundaries of a discrete-fracture network model take the form of arbitrary polyhedra. In general these may include an external boundary, which bounds the domain to be modelled, and an arbitrary number of internal boundaries which represent tunnels, segments of borehole, *etc*. Boundary conditions are imposed at intersections between discrete features and the external or internal boundaries.

Groundwater flow and transport through the discrete-fracture network are specified by 2-D equations that apply locally within each planar segment, by conditions of continuity which apply at the intersections between segments, and by the external and internal boundary conditions. The groundwater flow field is defined only on this network, and boundary conditions are specified only along the intersections between the network and the internal and external boundaries.

2.1.1 Deterministic structures

Site characterization at both Laxemar and Forsmark has identified a set of deformation zones on the scale of >1 km. These are treated as deterministic structures in the present study. That is, each realization of the model has these in the same positions. The deterministic structures are represented as piecewise planar transmissive features in the discrete-feature model.

The ground surface topography is represented as a distinct type of deterministic feature, which serves both as a transmissive feature (representing the permeability of the Quaternary cover and near-surface sheeting joints) and as a locus of points for imposing the surface boundary conditions (see Section 2.1.6). This "topographic feature" is defined for each site as a triangular network which is derived from the digital elevation models or contour maps as available.

2.1.2 Stochastic fractures

Fractures and minor deformation zones smaller than the 1 km scale are characterized in statistical terms, as a discrete-fracture network (DFN) submodel which forms a stochastic component of the discrete-feature model. Stochastic realizations of the DFN component are generated by simulation, using a different seed value for the random number generator to produce each realization. The DFN submodel for each site is defined in terms of statistical distributions of fracture properties (location, size, orientation, transmissivity etc.) for 4 to 5 sets of fractures within each rock domain. These statistical distributions are described in Sections 3.2.2 and 3.3.2 for Laxemar and Forsmark, respectively.

2.1.3 Equivalent features for block-scale representation

The DFN submodel would contain many millions of fractures if it were explicitly represented over the entire domain of the site-scale model, and this would lead to an intractably large network problem for numerical solution. In order to reduce the complexity of the problem, block-scale features are used to represent the contribution of smaller-scale fractures to large-scale flow, if these fractures are not in the immediate vicinity of the repository tunnels or deposition holes. The properties of these block-scale features are derived as follows.

Fractures that should be represented explicitly in the model are identified as a site-specific function of fracture size, fracture transmissivity, and distance to the repository volume. The distance from a fracture to the repository volume is evaluated as d_{min}, the minimum three-dimensional distance from any point on the fracture to any point on a polygon in the plane of the repository, which circumscribes one of the repository panels (Figure 2.1). Successively smaller and/or less transmissive fractures are retained explicitly for smaller values of d_{min}.

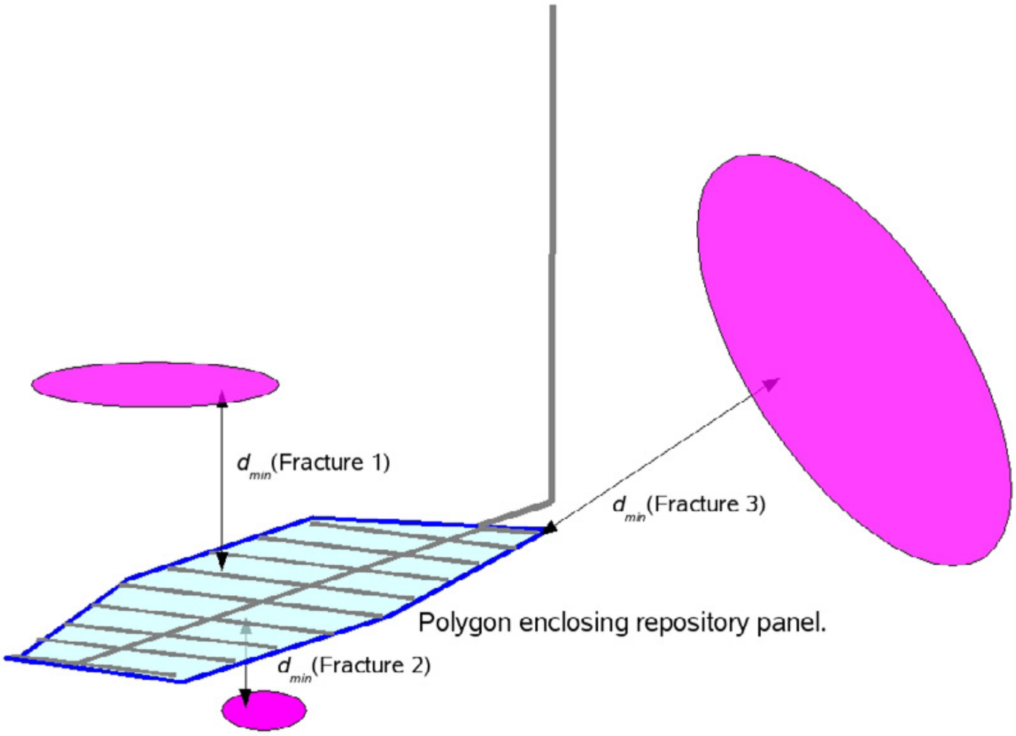

Figure 2.1. *Illustration of the minimum distance d_{min} from a given fracture to the polygon enclosing a repository panel in the horizontal plane, which is used as criterion for deciding which fractures should be retained explicitly in the model, versus which fractures should be represented in terms of aggregate block-scale properties.*

Fractures that are not represented explicitly in the model are considered to contribute to the 3-D hydraulic conductivity tensor **K** of the rock block that contains them. The contribution of a single fracture *i* to the block-scale tensor **K** is calculated from Snow's law (Snow, 1969) which can be written in matrix form as:

$$\mathbf{K}_i = \frac{T_i}{s_i}\left[\mathbf{I} - \vec{n} \otimes \vec{n}\right]$$

where:

T_i = fracture transmissivity

s_i = effective fracture spacing

I = the identity matrix with components $I_{ii} = 1$; $I_{ij} = 0$ for $i \neq j$; $i,j = 1,2,3$,.

$\vec{n}$ = unit normal vector to fracture plane

and where $\vec{n} \otimes \vec{n}$ denotes the outer (tensor) product with components $n_i n_j$, for $i, j = 1, 2, 3$.

The effective fracture spacing s_i is taken as V/A_i where A_i is the area of the fracture that lies within the volume V of the rock block (the entire area of the fracture, if the fracture is entirely within the rock block).

The block-scale hydraulic conductivity tensor is then approximated as the sum of the contributions of each fracture that has some portion within the block volume V:

$$\mathbf{K} = \sum_{i \in V} \mathbf{K}_i$$

Note that this approximation generally overestimates the block-scale hydraulic conductivity that would be obtained by an explicit block-scale DFN calculation (such as is performed in the CONNECTFLOW software used by SR-Can), since not all fractures within a given volume will form part of the conductive "backbone" of the through-flowing network, and the effects of network tortuosity are neglected. The approximation is used to reduce the computational burden, and is equivalent to that used in the DarcyTools software that has been used in SKB's site-descriptive modelling.

Block-scale porosity is calculated as a scalar property:

$$\Theta = \sum_{i \in V} \frac{b_i}{s_i}$$

where b_i is the effective transport aperture of the ith fracture. Note that this does not take into account possible directional dependence of block-scale porosity, which would require further development of the algorithms to evaluate.

Block-scale specific storage is calculated by an analogous formula:

$$S_s = \sum_{i \in V} \frac{S_i}{s_i}$$

where S_i is the storativity of the ith fracture. This is not used in the present study since only steady-state calculations are performed, but is mentioned for the sake of completeness.

Each rock block is then represented in the discrete-feature model by a set of three orthogonal features, which are divided into patches of different properties as illustrated in Figure 2.2. The transmissivities of the patches on the features are calculated by Newton-Raphson inversion to reproduce the diagonal components of the hydraulic conductivity tensor K_{11}, K_{22}, and K_{33} (see Geier, 2008 for details). Note that the off-diagonal components of the tensor $\mathbf{K}$ are not reproduced, so this representation results in some under-representation of anisotropy and reduction of the overall conductivity. These effects may are counter to the effects of the Snow's law approximation which is used to estimate K, so these are offsetting effects, but the net consequences have not been investigated.

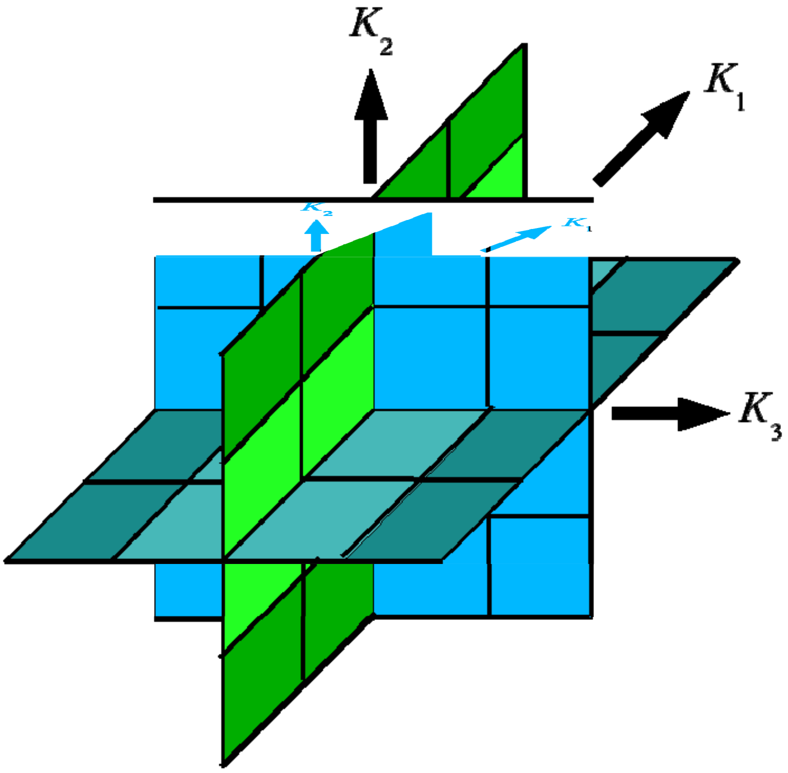

Figure 2.2 *Representation of a rock block by three orthogonal features to represent block-scale hydrologic properties in the discrete-feature conceptual model.*

2.1.4 Representation of repository tunnels and excavation-damaged zone

The hydraulic conductivity of backfilled tunnels and the transmissive excavation-damaged zone (EDZ) in the wall rock along repository tunnels are represented by transmissive features configured as a tube of rectangular cross-section, along the length of each tunnel segment (Figure 2.3). Repository access tunnels (main tunnels and transport tunnels) as well as deposition tunnels are represented in this fashion. These tubes are slightly larger than the actual tunnels (by 1 m on each side), to account for the extent of the excavation-disturbed zone (EDZ) into the wall rock. Transmissivity and aperture values are assigned to these features such that the total conductance of the tunnel cross section is reproduced. The parameters used to define these features are listed for Laxemar and Forsmark in Table 2.1.

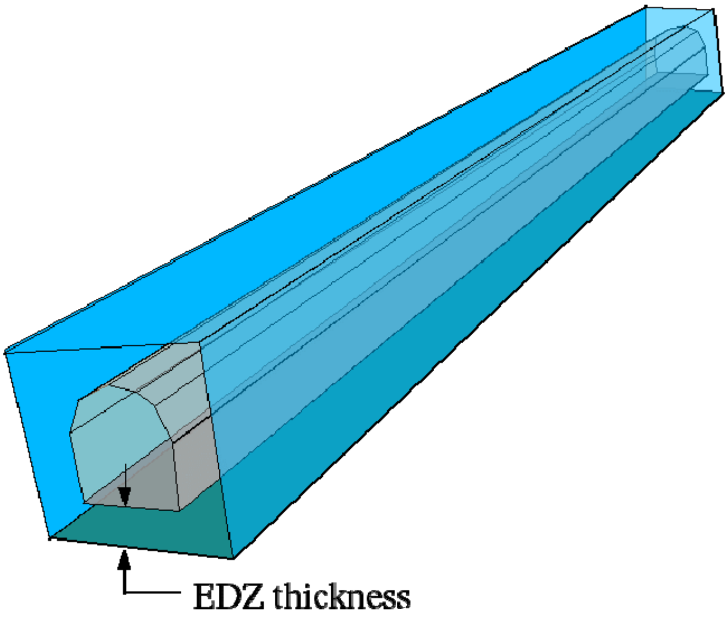

Figure 2.3 *Discrete-feature representation of repository tunnels and EDZ.*

Table 2.1 *Tunnel system parameters used in repository module. Sources for tunnel parameters are indicated by footnotes as listed at the bottom of the table.*

	Laxemar	Forsmark
Tunnel sides (rectangular approximation)	4	4
Tunnel floor[1,2]	-500 m	-410 m
Access tunnel height[3]	7 m	7 m
Access tunnel width[3]	7 m	7 m
Deposition tunnel width[3]	4.9 m	4.9 m
Deposition tunnel height[3]	5.4 m	5.4 m
EDZ thickness[4]	1 m	1 m
EDZ transmissivity[4]	5×10^{-7} m^2/s	5×10^{-7} m^2/s
EDZ storativity[4]	1×10^{-8}	1×10^{-8}
EDZ aperture[4]	2×10^{-5} m	2×10^{-5} m

[1] D1 repository design for Laxemar (Janson *et al.*, 2006)
[2] D1 repository design for Forsmark (Brantberger *et al.*, 2006)
[3] SR-Can Initial State Report (SKB, 2006d), Table 2-1.
[4] Assumed values corresponding to an EDZ composed of a continuous moderate-transmissivity fracture with effectively a cubic-law aperture (conservative values).

2.1.5 Canister emplacement criteria

Canister positions along the deposition tunnels are chosen for each realization of the discrete-fracture network, according to the full-perimeter intersection criterion (FPC) as described in the SR-Can Main Report and by Munier et al. (2006). This is done with the program *repository* which is part of the *dfm* toolkit.

For each deposition tunnel, full-perimeter intersections (FPIs) are identified as the simulated fractures that cross all surfaces (top, bottom, and sides) of the tunnel. Deposition hole positions are then chosen sequentially by the following procedure, avoiding positions in which the canister would be intersected by an FPI fracture:

Starting from the entrance of the deposition tunnel, the first part of length l_{plug} is avoided (see Figure 2.4) in order to allow room for a sealing plug, as specified in the D1 repository design (Janson *et al.*, 2006; Brantberger *et al.*, 2006).

A trial position is tested to see if:

1) it meets respect-distance criteria for any nearby deterministic deformation zones,

2) it meets the FPC criterion (i.e., no intersections with a FPI fracture) and,

3) (optionally) to see if the total transmissivity of fractures intersected by a pilot hole would be less than the allowable transmissivity.

If the trial position is acceptable, a deposition hole is created at the position and a new trial position is chosen a distance $l_{spacing}$ further along the tunnel, where $l_{spacing}$ is the design spacing between canisters, based on thermal criteria.

If the trial position is rejected, a new trial position is chosen by advancing a small distance l_{step} along the tunnel and repeating the tests, until an acceptable position is found.

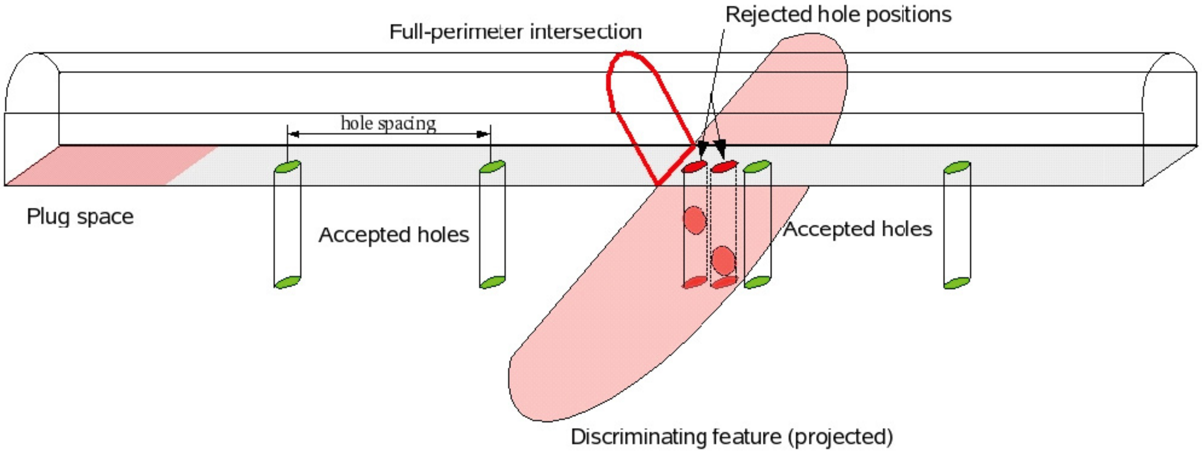

Figure 2.4 *Illustration of method for selecting deposition-hole positions, with accepted positions in green and rejected positions (due to FPC criterion) in red. The shaded area at the left side of the figure represents the space reserved for a plug at the start of the tunnel.*

The deposition holes for accepted position are represented by vertical, internal boundaries of hexagonal cross-section, starting from the floor of the tunnel and extending to the depth specified in the design. See Table 2.2 for deposition hole parameters based on the site-specific designs.

The deposition-tunnel utilization factor ϵ is calculated as:

$$\varepsilon = \frac{N_{accept} l_{spacing}}{\sum_i L_{usable,i}}$$

where N_{accept} is the number of accepted positions and $L_{usable,i}$ is the "usable" length of the ith deposition tunnel, after subtracting the portions that are reserved for the plug at the start and for clearance at the blind end of each tunnel.

Table 2.2 *Deposition hole parameters for the models. Sources for deposition-hole parameters are indicated by footnotes as listed at the bottom of the table.*

Deposition hole sides (hexagonal approximation to circle)	6
Deposition hole radius[1]	0.88 m
Deposition hole depth[1]	7.83 m
Canister radius[1]	0.53 m
Canister length[1]	4.83 m
Canister top[1]	2.5 m
Distance between holes $L_{spacing}$	7.8 m
Distance from drift end [3]	20 m
Distance from drift start L_{plug}[3]	8 m
Minimum step distance L_{step}[4]	1 m
Pilot hole transmissivity[4]	1×10^{-5} m^2/s

[1] SR-Can Initial State Report (SKB, 2006d), Figure 5-3.
[2] Based on D1 repository design for repository design for Laxemar (Janson *et al.*, 2006).
[3] Deep Repository, Underground Design Premises D1/1 (SKB, 2004).
[4] Assumed generic values.

2.1.6 Implementation of boundary conditions

The external boundary of each model is a box with rectangular sides. Boundary conditions are imposed at intersections between discrete features and the sides of this box (lower and lateral boundary segments), as well as at the nodes (vertices) of the topographic feature at the upper surface.

Two types of external boundary condition are imposed, depending on the site-specific model and variant:

- Specified head, where the head *h* is specified at each node on the boundary segment.

- Specified flux, where the flux *q* is specified at each node (most commonly $q = 0$ for no-flow boundaries).

- Deposition holes are represented as internal boundaries. The types of boundary conditions imposed on these internal boundaries may be either of two forms, depending on the model variant:

- Specified flux with $q = 0$ (no-flow) to represent a bentonite-filled deposition hole where flow is primarily around the hole.

- Specified net flux with $\sum q_i = 0$ and $h_i = h_b,\ i \in b$ to represent the case where bentonite is essentially eroded away so water flows freely through the deposition hole and heads around the boundary are essentially uniform.

2.1.7 Model assembly

For each realization of the stochastic DFN submodel, the discrete-feature model is assembled from a set of "panel" files that describe the geometry of the components described in the foregoing sections:

- Outer boundary
- Topography
- Deterministic deformation zones
- Stochastic realization of the DFN population (retained features)
- Equivalent features for block-scale representation of stochastic fractures that are not explicitly retained.
- Repository tunnel/EDZ features,
- Deposition holes conditioned on the DFN realization.

A finite-element mesh is produced by finding all intersections among these features, then triangulating each feature (Figure 2.5) so that the geometry is defined by a series of nodes (vertices with 3-D coordinates) and triangular elements, each with transmissivity, transport aperture , and storativity corresponding to the feature from which they were derived. This is accomplished by the program *meshgenx*, which is part of the *dfm* toolkit (Appendix A; Geier 2005; Geier, 2008).

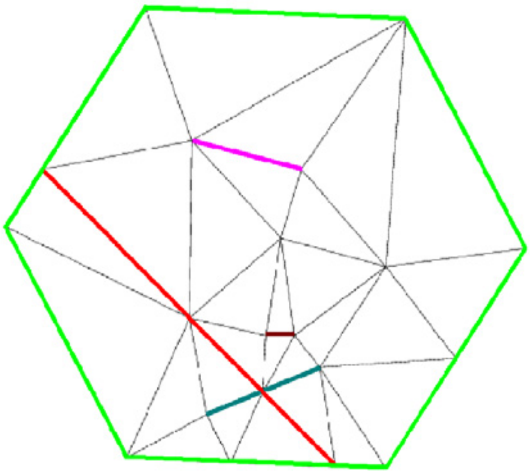

Figure 2.5 *Example of discretization of a hexagonal feature into triangular elements, constrained by intersections with other features (represented by the thicker, coloured lines).*

2.2 *Flow and transport modelling*

2.2.1 Flow equations and method of solution

Within each planar segment of a feature, groundwater flow is governed by the 2-D transient flow equation:

$$S \frac{\partial h}{\partial t} \quad - \quad \nabla \cdot (T \, \nabla h) \quad = \quad q(\vec{\xi})$$

where S and T are respectively the local storativity and transmissivity, h is hydraulic head, t is time, and q is a source/sink term which is zero everywhere except at the specified boundaries. In the present work, S and T are assumed to be homogeneous within a given triangular segment. Conservation of mass and continuity of hydraulic head are required between segments, and at intersections between features.

All cases modelled in this study are for steady-state flow, in which case the time derivative is zero and the local flow equation simplifies to

$$\nabla \cdot (T \nabla h) \quad = \quad -q(\vec{\xi})$$

To solve the flow equations for a given realization of a discrete-fracture network model, the network is discretized to form a computational mesh, which consists of 2-D, triangular finite elements that interconnect in 3-D. The head field is calculated by the Galerkin finite-element method. For the case of steady-state flow this leads to a system of linear algebraic equations of the form:

$$\mathbf{A}\vec{h} = \vec{q}$$

where **A** is a sparse, diagonally dominant, banded matrix with coefficients depending only upon the transmissivity and geometry of each triangular element, $\vec{h}$ is a column vector of steady-state head values at the element vertices, and $\vec{q}$ is a column vector of unbalanced flux values at the vertices, equal to zero except at physical boundaries where inflow or outflow occurs. Details of the derivation are given by Geier (2005).

Features that are not connected to a specified-head boundary (either directly or indirectly via connections with other features and/or net-specified-flux boundaries) are indeterminate and are not represented in the matrix equations. These features constitute hydraulically isolated networks.

Solutions to the systems of linear algebraic equations for the steady-state case are obtained using standard sparse-matrix methods (conjugate-gradient method preconditioned by simple diagonal scaling of incomplete Choleski factorization, depending on the calculation case), as implemented in the *dfm* code.

2.2.2 Particle tracking to characterize transport paths

To characterize transport paths, advective-dispersive transport of nonsorbing solute in the 3-D network (for the case of no matrix diffusion) is modelled by the discrete-parcel random walk (DPRW) method (Ahlstrom *et al.*, 1977), as implemented in the *meshtrkr* module of the *dfm* toolkit (Geier, 2005; Geier, 2008). This approach represents local, 2-D advective-dispersive transport within each fracture plane. 3-D network dispersion, due to the interconnectivity among discrete features, arises as the result of local dispersion in combination with mixing across fracture intersections.

Particles are initiated at source locations. In the present study, the sources are considered to be the perimeters of the deposition holes, which are internal boundaries to the mesh as described in Section 2.1.6. Particles are initiated along the line segments where fractures intersect the holes, at randomly distributed locations along the segments.

Once inside the mesh, the motion of a particle within a fracture element (triangular finite element) is modelled as a random walk within the fracture plane. In the random walk, each step $\Delta \vec{x}$ consists of a deterministic, advective component plus a random, dispersive component:

$$\Delta\vec{x} \quad = \quad \vec{v}\Delta t + \quad \vec{r}$$

where Δt is a locally-specified time step, $\vec{v} = -\frac{T}{b_T}\nabla h$ is the (local) fluid velocity within the plane of the element, T is the local transmissivity, b_T is the local effective transport aperture, ∇h is the 2-D head gradient within the plane of the element, and $\vec{r}$ is the vector sum of random components representing longitudinal and transverse dispersion:

$$\vec{r} \quad = \quad r_L\vec{u}_L \quad + \quad r_T\vec{u}_T$$

where $\vec{u}_L = \vec{v}/\|\vec{v}\|$ is the unit vector parallel to the local velocity and $\vec{u}_T \quad = \quad \vec{n}\times\vec{u}_L$ (where $\vec{n}$ is the unit normal to the element plane) is a unit vector transverse to the local velocity, within the plane of the element. The random scalars r_L and r_T (with dimensions of length) are drawn from normal distributions with zero mean:

$$r_L \quad \sim \quad N\left(0, \sqrt{2D_L\Delta t}\right)$$

$$r_T \quad \sim \quad N\left(0, \sqrt{2D_T\Delta t}\right)$$

where D_L is the longitudinal dispersion coefficient and D_T is the transverse dispersion coefficient.

The local dispersion coefficients depend on the magnitude of the local velocity as:

$$D_L = \alpha_L |\vec{v}| + D_m$$

$$D_T = \alpha_T |\vec{v}| + D_m$$

where α_L and α_T are the longitudinal and transverse dispersivities, respectively, within a given fracture.

Application of the DPRW model in a network requires an assumption regarding the degree of mixing within each fracture intersection, due to molecular diffusion across streamlines as water passes through the intersection. The degree of mixing in an intersection is governed by the Peclet number for flow through the intersection:

$$Pe = \frac{vb}{D_d}$$

where b is the fracture aperture, v is the mean fluid velocity and D_d is the coefficient of molecular diffusion. Berkowitz *et al.* (1994) showed that for an idealized intersection, mixing is negligible for $\mathrm{Pe} > 0.1$, but significant for $\mathrm{Pe} = 0.0001$, which corresponds to $v \approx 3$ cm/yr in a 0.1 mm fracture. For natural gradients that are expected within a radioactive-waste repository, v can be on the order of 1 m/yr or less, and substantial mixing will occur at most fracture intersections.

Hence complete mixing is assumed as a reasonable approximation in this study. When a particle arrives at an intersection edge, the particle is randomly assigned to one of the elements sharing that edge. The probability of assignment to the *i*th connected element is:

$$\mathrm{P}[\,i\,] = \mathrm{Q}_i / \sum_e \mathrm{Q}_e$$

where Q_e is the inflow to the *e*th connected element along the edge (zero if there is outflow), and the summation is taken over all elements connected to the edge. This reassignment technique does not allow for particles to move between adjacent elements in the absence of net advection.

Hence the model may under-represent the actual diffusion and/or transverse dispersion (due to small-scale heterogeneity within fracture planes) that takes place in the physical system.

2.2.3 Calculation of pathway parameters

Advective-dispersive particle trajectories are traced for multiple particles for each deposition hole in the repository. For each release-path trajectory $\vec{\tau}$ consisting of discrete segments $\{\tau_1, \tau_2, ...\}$ the following quantities are calculated by summing over the segments τ_i :

$$
\begin{aligned}
F_r &= \sum_{\tau_i} \frac{a_w(\tau_i)\Delta l}{v(\tau_i)} = \sum_{i} \frac{2\Delta t}{b_T(\tau_i)} \\
L_r &= \sum_{\tau_i} \Delta l \\
t_r &= \sum_{\tau_i} \Delta t \\
I_a &= \sum_{\tau_i} a_w(\tau_i)\Delta l = \sum_{\tau_i} \frac{2\Delta l}{b_T(\tau_i)} \\
I_b &= \sum_{\tau_i} b_T(\tau_i)\Delta l \\
I_c &= \sum_{\tau_i} T(\tau_i)\Delta l
\end{aligned}
$$

where Δl and Δt are the increments of distance and time for each step, $a_w = 2/b_T$ is the local wetted surface per unit volume water, T is the local transmissivity, and $v = \Delta l/\Delta t$ is the magnitude of the local advective velocity. The same quantities are also calculated for each class of features Φ along each path:

$$
\begin{aligned}
F_{r\Phi} &= \sum_{\tau_i \in \Phi} \frac{2\Delta t}{b_T(\tau_i)} \\
L_{r\Phi} &= \sum_{\tau_i \in \Phi} \Delta l
\end{aligned}
$$

$$t_{r\Phi} = \sum_{\tau_i \in \Phi} \Delta t$$

$$I_{a\Phi} = \sum_{\tau_i \in \Phi} \frac{2\Delta l}{b_T(\tau_i)}$$

$$I_{b\Phi} = \sum_{\tau_i \in \Phi} b_T(\tau_i)\Delta l$$

$$I_{c\Phi} = \sum_{\tau_i \in \Phi} T(\tau_i)\Delta l$$

The location local fluid velocity, and aperture at the source are also recorded, along with the exit location which can subsequently be related to the biosphere receptor (lake, sea, mire etc.) in the landscape for risk calculations. For detailed models of transport along streamlines, the properties of features traversed by each particle are also recorded.

In some calculation cases the excavation-disturbed zone (EDZ) around the deposition tunnels forms an important path for transport. Hence particles released from a source S_i at one deposition hole may travel along the tunnel and arrive another deposition hole S_j before they continue along the way to the surface. The properties of the release paths represented by such particles can be found by convolution of the distributions of properties for paths from S_i to S_j with the distributions of paths S_j from to the surface.

3 Definition of calculation cases for SR-Can review

The models for the following calculations are discrete-feature implementations of SKB's Site Descriptive Model (SDM) 1.2, for the Laxemar and Forsmark sites respectively. Post-closure, saturated conditions are assumed unless otherwise noted. Alternative interpretations of the model components, such as large-scale deformation zones (DZs) or the near-field discrete-fracture network (DFN), and alternative boundary conditions are treated as variations.

The models include site-specific representation of the repository layout according to SKB's D1 design. Backfill, buffer, and excavation-damage zone (EDZ) permeabilities for the base case are represented as equivalent discrete-features according to design specifications. Deposition holes are placed consistent with SKB's criteria for avoiding discriminating fractures. Deviations from the design properties due to effects such as spalling or shear displacements, or due to possible errors in applying the discriminating-fracture criteria, are considered as variations.

The base case model for each site represents late-temperate conditions, with flow simply in response to topographic gradients (though the influence of salinity is not taken into account).Variants (for Forsmark only, to date) consider the effects of alternative hydrologic properties in the large-scale features, different temperate-climate regimes, and stress-induced spalling around deposition holes. Variants to explore future glacial climate scenarios were not completed by the time of this report, and will be presented in a subsequent report. The variants that were modelled for Forsmark are summarized in Table 3.1.

Table 3.1 *Summary of model variants for Forsmark.*

Variant code	Brief description	Climate setting	Deformation-zone transmissivity	Spalling
cT	Base case	Late-temperate (*ca.* 9000 CE)	SDM 1.2 best estimates	None
c	Uniform DZ *T*	Late-temperate (*ca.* 9000 CE)	Uniform	None
cTS	Mid-temperate	Mid-temperate (present-day)	SDM 1.2 best estimates	None
cspT	Basic spalling	Late-temperate (*ca.* 9000 CE)	SDM 1.2 best estimates	On all sides of deposition holes
cspT	Directional spalling	Late-temperate (*ca.* 9000 CE)	SDM 1.2 best estimates	On deposition-hole sides facing direction of minimum horizontal stress.

3.1 Sources of data

The main sources of site-specific data for the models are the Site Descriptive Models (SDMs), version 1.2, for the Forsmark and Laxemar sites, as described in the SDM v. 1.2. reports (SKB 2005 and 2006a, respectively), and supporting reports as referenced therein, most importantly the analyses of fracture data (SKB 2006c and Hermanson et al., 2005) and regional and site-scale hydrogeologic modelling (Follin et al., 2005; Hartley et al., 2006abc).

Information on the repository designs for SR-Can are taken from the SR-Can Main Report (SKB 2006b) and the SR-Can Data Report (SKB, 2006c), and from the D1 design reports (Brantberger et al., 2006 and Janson et al., 2006).

In general, the approach has been to adopt SKB's descriptions directly for the base-case models, without introducing other information that has been developed in the course of Field Technical Reviews or other review activities of SKI's INSITE review group, although such information may inform the selection of scenarios for ongoing calculations.

3.2 Discrete-feature model for Laxemar

The discrete-feature model and variants for Laxemar are defined in terms of local coordinates:

$$\begin{aligned} x &= X - X_o \\ y &= Y - Y_o \\ z &= Z - Z_o \end{aligned}$$

where the origin of the local coordinate system used is at X_o = 1540000 RAK, Y_o = 6360000 RAK, Z_o = mean sea level.

The domain boundaries for the Laxemar model are defined as follows:

East boundary at X = 1 554 000 RAK (x = 14 000 m).
West boundary at X = 1 547 000 RAK (x = 7 000 m).
South boundary at Y = 6 365 000 RAK (y = 5 000 m).
North boundary at Y = 6 368 200 RAK (y = 8 200 m).
Lower boundary at Z = -1950 m.a.s.l. (z = -1 950 m)

3.2.1 Deformation zones

Large-scale deformation zones at Laxemar are represented explicitly in the model as deterministic features, based on the maps and estimates of properties presented in SKB (2006a) and Hartley et al. (2006c).

Alternative structural interpretations have not been modelled in the present study, due to time limitations. Deformation zones are treated as having homogeneous hydraulic properties; the case of deformation zones with heterogeneous properties is another important possibility which has not been modelled here.

3.2.2 Fracture population statistics

The fracture population for the Laxemar model is simulated based on the statistical hydro-DFN model specified in SKB (2006a) Tables 8-19, 8-20 and 8-21 which are equivalent to Hartley et al. (2006c) Tables 3-22, 3-23 and 3-24. Fracture sets are defined separately for (1) Rock Domain A, (2) Rock Domains B & C, and (3) Rock Domains M(A), M(D) and D. For each of these, separate statistics are given for upper ($z > -300$ m) and lower ($z >= -300$ m) domains. Fracture set definitions files used as input to the *dfm* module *fracgen*, for these six parts of the model volume, are included on an accompanying CD-ROM.

One significant adaptation of the SR-Can hydro-DFN models was made for Laxemar, to help produce better-conditioned mesh geometry for *dfm* calculations. Discrete directional distributions were used for fracture orientation, rather than the continuous directional distributions that were used in SR-Can. The discrete distributions are generated as follows: After simulating a fracture pole (*i.e.* normal vector) $\vec{n}$ from the specified distribution for a given rock domain and fracture set (in general, a Fisher distribution), this is replaced by the vector $\vec{n}_I$ from an equally-distributed, icosahedral set $\{\vec{n}_1, \vec{n}_2, \ldots, \vec{n}_{20}\}$, such that $\vec{n}_I$ maximizes $\vec{n} \cdot \vec{n}_I$.

This method produces the same number of fracture poles within each icosahedral sector of the sphere, as for the specified continuous distribution. Hence it is expected to produce anisotropic connectivity and flow very similar to the fitted orientation distributions. However, it has the advantage of avoiding very-low-angle intersections which can lead to low-aspect and/or very obtuse triangular elements in the finite element mesh, and thus make numerical solution of the flow equations more difficult.

The fracture-generation domains are specified as a series of polyhedra corresponding to the boundaries of Rock Domain A, Rock Domains B&C, and Rock Domains D, E, & M (see accompanying CD). For each realization, the DFN fractures are generated for all domains simultaneously, so that truncation effects between domains are avoided.

In order to reduce the complexity of the finite-element problem, runs were performed for three sections of the repository, in each case simulating all of the fractures but keeping the detailed representation only around part of the repository, while the remainder of the fractures contributed to the block-scale properties for the equivalent block-scale representation. The repository sections, labeled Section A, Section D, and Section E, are defined in Section 3.2.4.

In each case, fractures are either retained explicitly or assigned to the block-scale features, depending on their proximity to polygons bounding these sets of repository panels (defined in the "sites" files listed in the accompanying CD-ROM) in combination with their size and transmissivity. The rules for retaining fractures explicitly are specified in Table 3.2.

Table 3.2 *Rules for explicitly retaining fractures of a given radius* r_f *and transmissivity* T_f *when* d_{min} *is the minimum distance from any point on the fracture to the polygon enclosing the portions of the repository being modelled (see Figure 2.1 in Section 2.1.3), for the Laxemar model, as defined in the fracgen input file Laxemar500m_thin.shells. Note that no fractures are retained in the distance range specified for Shell 1, as the indicated values of* r_f *and* T_f *are never exceeded by the DFN statistical model.*

Shell	Distance range	Retain if r_f is greater than:	and T_f is greater than:
1	500 m < d_{min} ≤ 10000 m	10000 m	1×10^{10} m^2/s
2	100 m < d_{min} ≤ 500 m	250 m	1×10^{-5} m^2/s
3	50 m < d_{min} ≤ 100 m	100 m	1×10^{-5} m^2/s
4	20 m < d_{min} ≤ 50 m	50 m	1×10^{-6} m^2/s
5	10 m < d_{min} ≤ 20 m	25 m	3×10^{-6} m^2/s
6	5 m < d_{min} ≤ 10 m	10 m	1×10^{-6} m^2/s
7	2.5 m < d_{min} ≤ 5 m	5 m	1×10^{-7} m^2/s
8	0 < d_{min} ≤ 2.5 m	2 m	1×10^{-9} m^2/s

3.2.3 Repository layout

The layout for the Laxemar repository is based on the central layout at the z = -500 m level as defined by the D1 design report (Janson et al., 2006). The access tunnels and deposition tunnels included in the model are shown in Figure 3.1.

For purposes of simulation, the repository is modelled in separate runs for each of three different sections, defined as comprising the following parts of the repository. The sections correspond to the following repository panels:

Section A: Panels A, B, C, and D (southeast).
Section D: Panel D (northwest)
Section E: Panel E.

The full network of access tunnels is included for each section, but the deposition tunnels and fractures are simulated only for the section being modelled in a particular run.

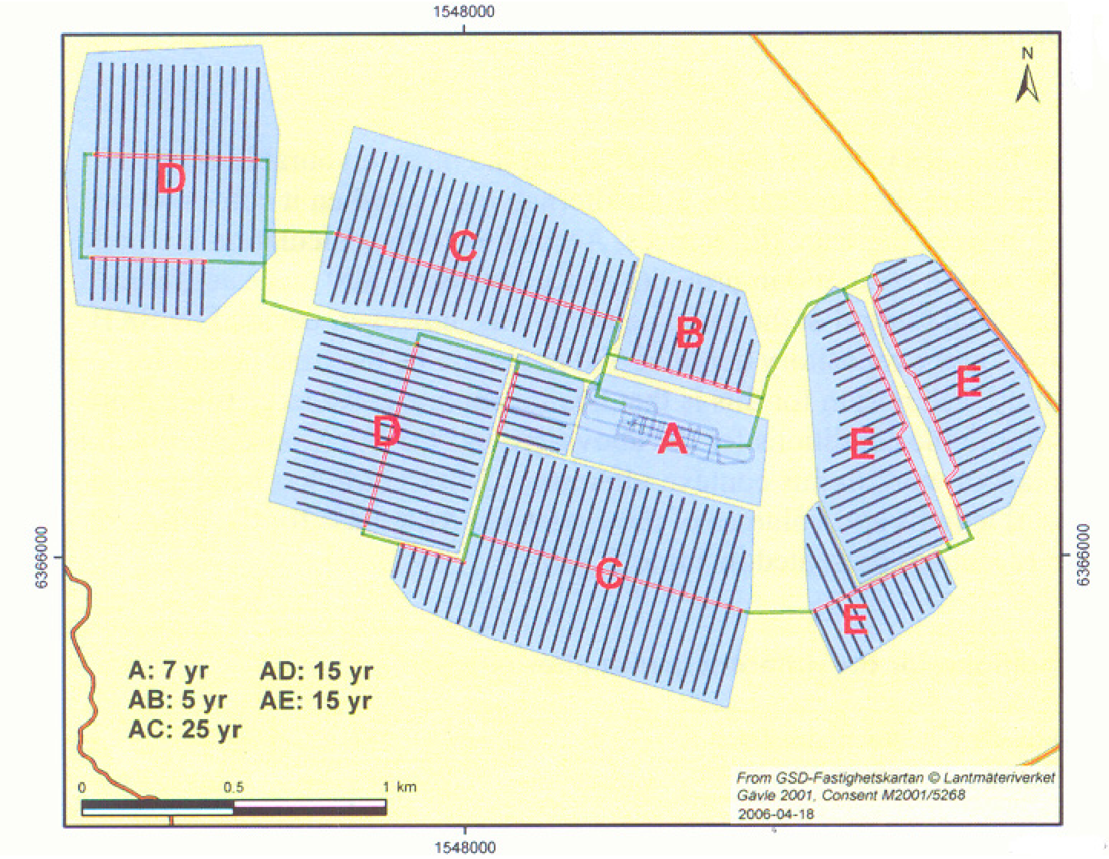

Figure 3.1 *Tunnel layout and construction sequence for Laxemar central layout (from D1 Design Report Janson et al., 2006, Figure 5-8).*

Figures 3.2 through 3.4 show the repository layouts for the three sections of the repository. The canister positions vary depending on the realization of the fracture network model, with application of the deposition-hole criteria. Those shown in the figure are for one particular realization of the model.

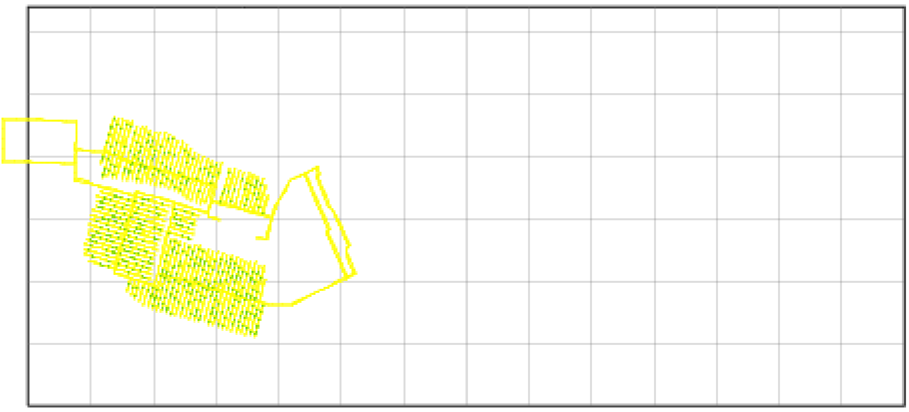

Figure 3.2 *Tunnel EDZ features and deposition holes for Laxemar repository Section A (Base Case Realization 01). EDZ features are indicated in yellow; deposition holes for positions that satisfy the deposition-hole criteria are in green. The grid (grey lines) is a reference grid with 0.5 km spacing, oriented N-S and E-W and corresponding to the Swedish Land Survey's RAK regional coordinate system. This grid is given in a consistent location in subsequent figures for ease of comparison of relative locations.*

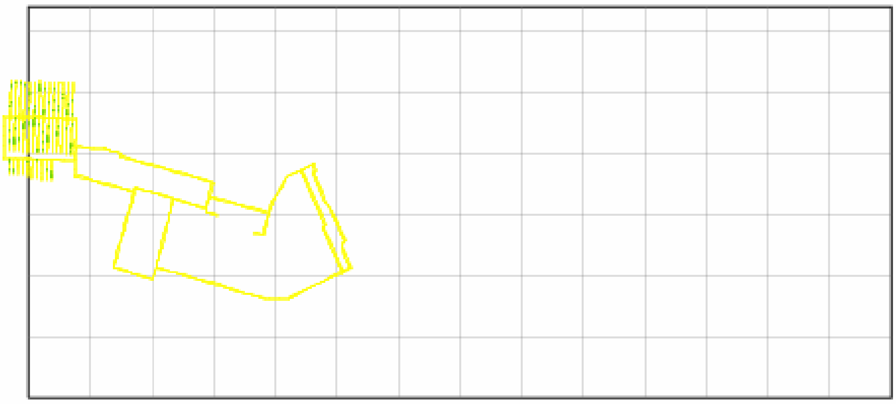

Figure 3.3 *Tunnel EDZ features and deposition holes for Laxemar repository Section D (Base Case Realization 01). EDZ features are indicated in yellow; deposition holes for positions that satisfy the deposition-hole criteria are in green.*

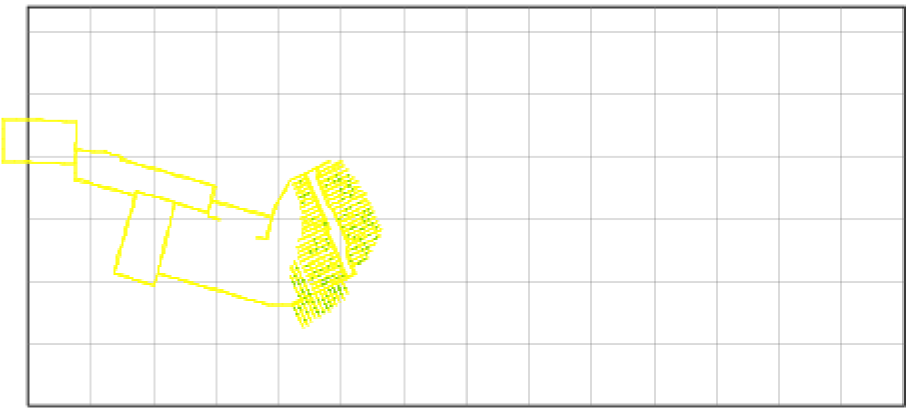

Figure 3.4 *Tunnel EDZ features and deposition holes for Laxemar repository Section E (Base Case Realization 01). EDZ features are indicated in yellow; deposition holes for positions that satisfy the deposition-hole criteria are in green.*

3.2.4 Nested model construction

The DFM model geometry for Laxemar is fully defined by the panel files that describe the components, as described in the foregoing sections. These components are first assembled in a single file which contains all of the geometric features in the model. Figure 3.5 shows an example for Section E of the repository.

3.2.5 Boundary conditions for temperate period

Boundary conditions for the base-case model represent flow simply in response to the topographic gradient. Since the topographic gradient at Laxemar is predominantly east-west, for the sake of simplicity this is accomplished by applying fixed heads at the west and east edges, with head values equal to the approximate elevations, and no-flow conditions along the north, south, and bottom sides (Table 3.3).

The upper surface of the model is assigned a head equal to the topographic elevation if on land, or zero for the portions of the model that represent the sea floor. In reality the groundwater pressures at the seabed will be higher due to the salinity of the water column, so this approach will somewhat exaggerate the pressure gradients (expressed as equivalent freshwater head) through the model.

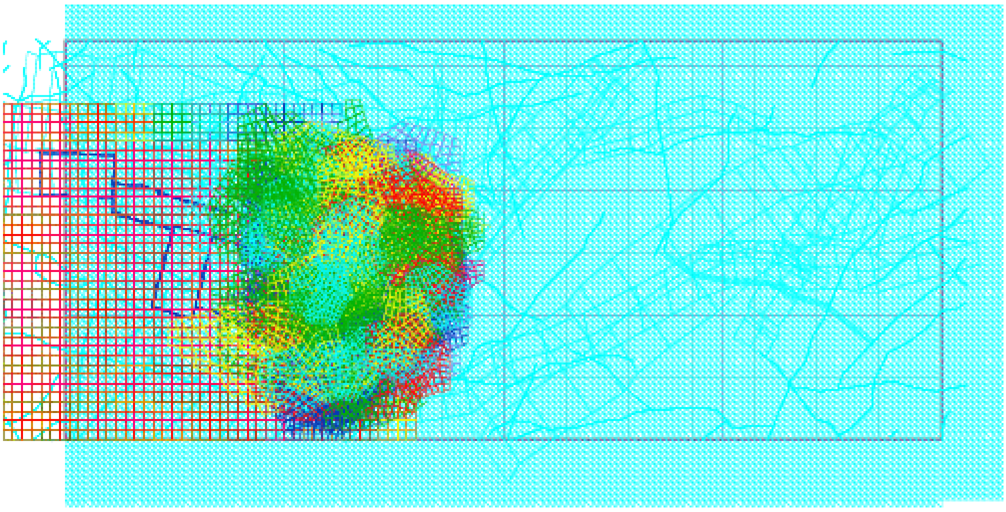

Figure 3.5 *Example of a composite panel file for the Laxemar base case model (Section E, Realization 1).*

***Table 3.3** External boundary conditions for the Laxemar base-case model.*

Boundary Segment	Type of boundary condition	Value(s)
South side	Specified flux	$q = 0$ (no flow)
East side	Specified head	$h = 0.4$ m
North side	Specified flux	$q = 0$ (no flow)
West side	Specified head	$h = 14.5$ m
Bottom	Specified flux	$q = 0$ (no flow)
Surface	Specified head	$h = z$
Sea floor	Specified head	$h = 0$

3.2.6 Boundary conditions during glacial retreat

Glacial retreat following the future glaciations is expected to produce the most extreme hydraulic head gradients during the functioning life of the repository, due to glacial meltwaters at the base of the retreating glaciers. These meltwaters may have a high dissolved oxygen content. Their potential to penetrate to repository depths is of concern since oxidizing conditions have the potential to affect engineered-barrier performance. In the event that canisters do fail, these high gradients also give the potential for relatively rapid transport to the surface, with accordingly low retention of radionuclides.

Boundary conditions for this case can be specified as an east-west gradient, with head on the west side of the model equal to the maximum expected thickness of the ice during glacial retreat, and head approximately equal to sea level on the east boundary. A head difference of 1000 m across the model is expected to be very conservative since most likely the ice front will be more gradual in slope, and since drainage by ice rivers at the base of the ice is expected to partly reduce the head.

Calculation cases for glacial retreat were not completed as of the date of this report, so these are not discussed further herein.

3.3 Discrete-feature model for Forsmark

The discrete-feature model and variants for Forsmark are defined in terms of local coordinates:

$$\begin{aligned} x &= X - X_o \\ y &= Y - Y_o \\ z &= Z - Z_o \end{aligned}$$

where the origin of the local coordinate system used is at X_o = 1630 000 RAK, Y_o = 6696 000 RAK, Z_o = mean sea level.

The domain boundaries for the Forsmark model are defined in terms of the local coordinates (x,y,z) as follows:

Southwest boundary: Line from (x = -4620 m, y = 3318 m) to (x = 3152 m, y = -4505 m)
Southeast boundary: Line from (x = 3152 m, y =-4505 m) to (x = 13826 m, y = 6170 m)
Northeast boundary: Line from (x = 13826 m, y = 6170 m) to (x = 5984 m, y = 13889 m)
Northwest boundary: Line from (x = 5984 m, y = 13889 m) to (x = -4620 m, y = 3318 m)
Lower boundary: z = -1950 m.

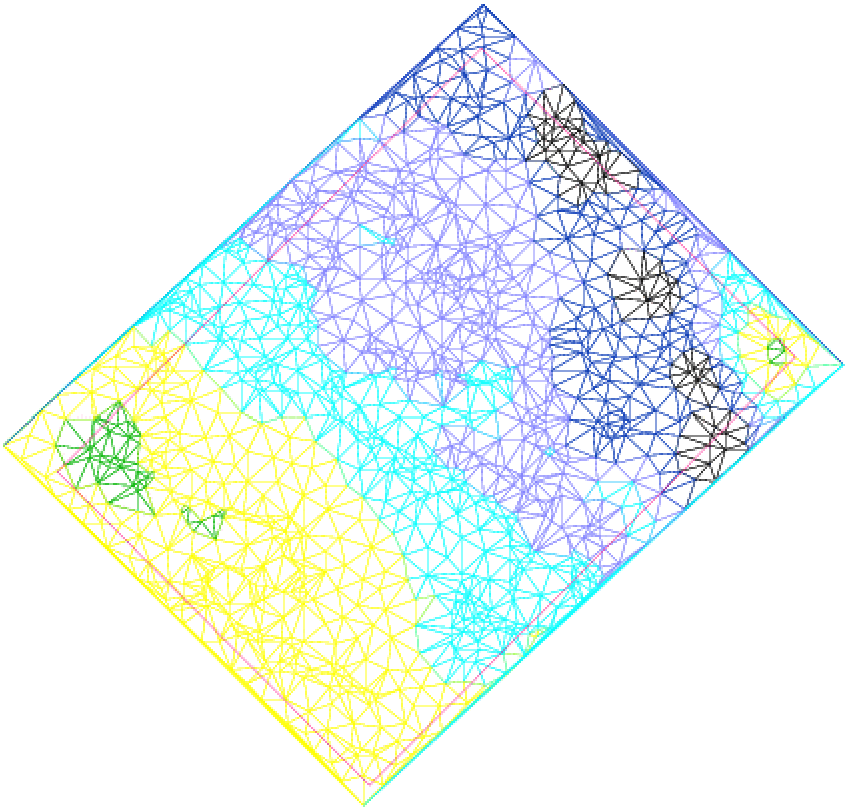

Figure 3.6 *Surface feature for the discrete-feature model of Forsmark, discretized as a triangular irregular network and colored to show topographic/bathymetric elevations (green is highest above sea level; black is deepest below sea level). The red rectangle shows the boundary of the modelled domain.*

3.3.1 Deformation zones

Hydraulic properties for the deformation zones in the base-case model were assigned based on SKB's HCD1 variant, which uses separate deterministic trends with depth.

For gently dipping and steeply dipping deformation zones the transmissivity (in units of m/s^2) is given by Eq 8-7a and 9-7b , respectively, in SKB (2005) as:

$$\begin{aligned} T_G(D) &= \max\left(4.1\cdot 10^{-4} e^{-0.0116D}, 1\cdot 10^{-8}\right) \\ T_S(D) &= \max\left(4.6\cdot 10^{-5} e^{-0.0174D}, 1\cdot 10^{-8}\right) \end{aligned}$$

where D is the depth (in meters).

The effective transport aperture b_T and storativity S are assumed to be correlated to transmissivity as:

$$b_T = 0.5\,T^{0.5}$$

$$S = 7 \cdot 10^{-4}\,T^{0.5}$$

consistent with Eq 8-9 and 8-11 in SKB (2005).

3.3.2 Fracture population statistics

The fracture population for the Forsmark model is simulated based on the statistical hydro-DFN model specified in SKB (2006a) Tables 8-19, 8-20 and 8-21 which are equivalent to Hartley et al. (2006c) Tables 3-22, 3-23 and 3-24. Fracture sets are defined separately for (1) Rock Domain A, (2) Rock Domains B & C, and (3) Rock Domains M(A), M(D) and D. For each of these, separate statistics are given for upper (z > -300 m) and lower (z >= -300 m) domains. Fracture set definitions files used as input to the *dfm* module *fracgen*, for these six parts of the model volume are included on the accompanying CD.

In each case, fractures are either retained explicitly or assigned to the block-scale features, depending on their proximity to polygons bounding these sets of repository panels (defined in the "sites" files in the accompanying CD) in combination with their size and transmissivity. The rules for retaining fractures explicitly are specified in Table 3.4.

The grid for the equivalent block-scale features covers the domain bounded by

East side at X = 1 638 000 RAK (x = 8 000 m).
West side at X = 1 627 000 RAK (x = -3 000 m).
South side at Y = 6 697 000 RAK (y = 1 000 m).
North side at Y = 6 703 000 RAK (y = 7 000 m).
Upper boundary at Z = 0 m.a.s.l. (z = 0 m).
Lower boundary at Z = -1 950 m.a.s.l. (z = -1 950 m).

Table 3.4 *Rules for explicitly retaining fractures of a given radius* r_f *and transmissivity* T_f *when* d_{min} *is the minimum distance from any point on the fracture to the polygon enclosing the portions of the repository being modelled (see Figure 2.1 in Section 2.1.3), for the Forsmark model. Note that no fractures are retained in the distance range specified for Shell 1, as the indicated values of* r_f *and* T_f *are never exceeded by the DFN statistical model.*

Shell:	Distance range	Retain if r_f is greater than:	and T_f is greater than:
1	$500\text{ m} < d_{min} \leq 50000\text{ m}$	10000 m	$1\times10^{10}\text{ m}^2/\text{s}$
2	$100\text{ m} < d_{min} \leq 500\text{ m}$	250 m	$1\times10^{-5}\text{ m}^2/\text{s}$
3	$50\text{ m} < d_{min} \leq 100\text{ m}$	100 m	$1\times10^{-5}\text{ m}^2/\text{s}$
4	$20\text{ m} < d_{min} \leq 50\text{ m}$	50 m	$1\times10^{-6}\text{ m}^2/\text{s}$
5	$10\text{ m} < d_{min} \leq 20\text{ m}$	25 m	$3\times10^{-6}\text{ m}^2/\text{s}$
6	$5\text{ m} < d_{min} \leq 10\text{ m}$	10 m	$1\times10^{-6}\text{ m}^2/\text{s}$
7	$2.5\text{ m} < d_{min} \leq 5\text{ m}$	5 m	$1\times10^{-7}\text{ m}^2/\text{s}$
8	$0 < d_{min} \leq 2.5\text{ m}$	2 m	$1\times10^{-9}\text{ m}^2/\text{s}$

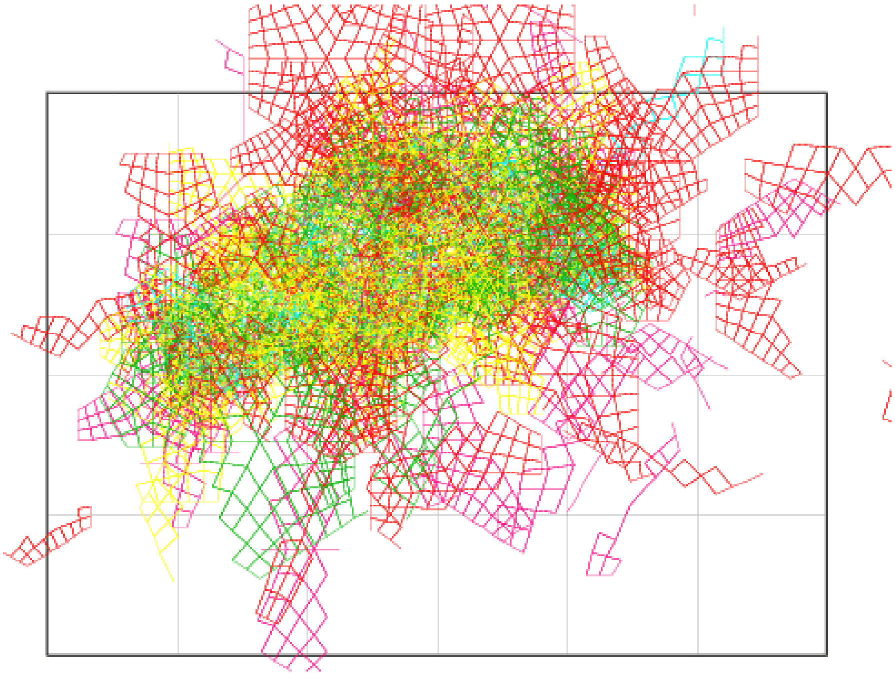

Figure 3.7 *Plan view of portion of stochastic fracture population (shown as wire frame view of edges of the quadrilateral panels that represent sections of each fracture) in slice -450 < z < -350 m retained for simulation of Section AC of the Forsmark repository. Red fractures are higher transmissivity; yellow, green and cyan are progressively lower-transmissivity. The jagged appearance of some fractures is due to panel edges being omitted if they are outside of the slice. The grid (grey lines) is a reference grid with 0.5 km spacing, oriented N-S and E-W, corresponding to the Swedish Land Survey's RAK regional coordinate system. This grid is given in a consistent location in subsequent figures for ease of comparison of relative locations.*

3.3.3 Repository layout

The layout for the Forsmark repository is based on the layout at the z = -410 m level as defined by the D1 design report (Brantberger *et al.*, 2006). The access tunnels and deposition tunnels included in the model are shown in Figures 3.8 and 3.9. For purposes of simulation, the repository is modelled in separate runs for each of three different sections, defined as comprising the following parts of the repository:

Section AC: Panels DEP 1 and DEP 3.
Section BD: Panels DEP 2 and DEP 4.
Section E: Panel DEP 5.

The full network of access tunnels is included for each section, but the deposition tunnels and fractures are simulated only for the section being modelled in a particular run.

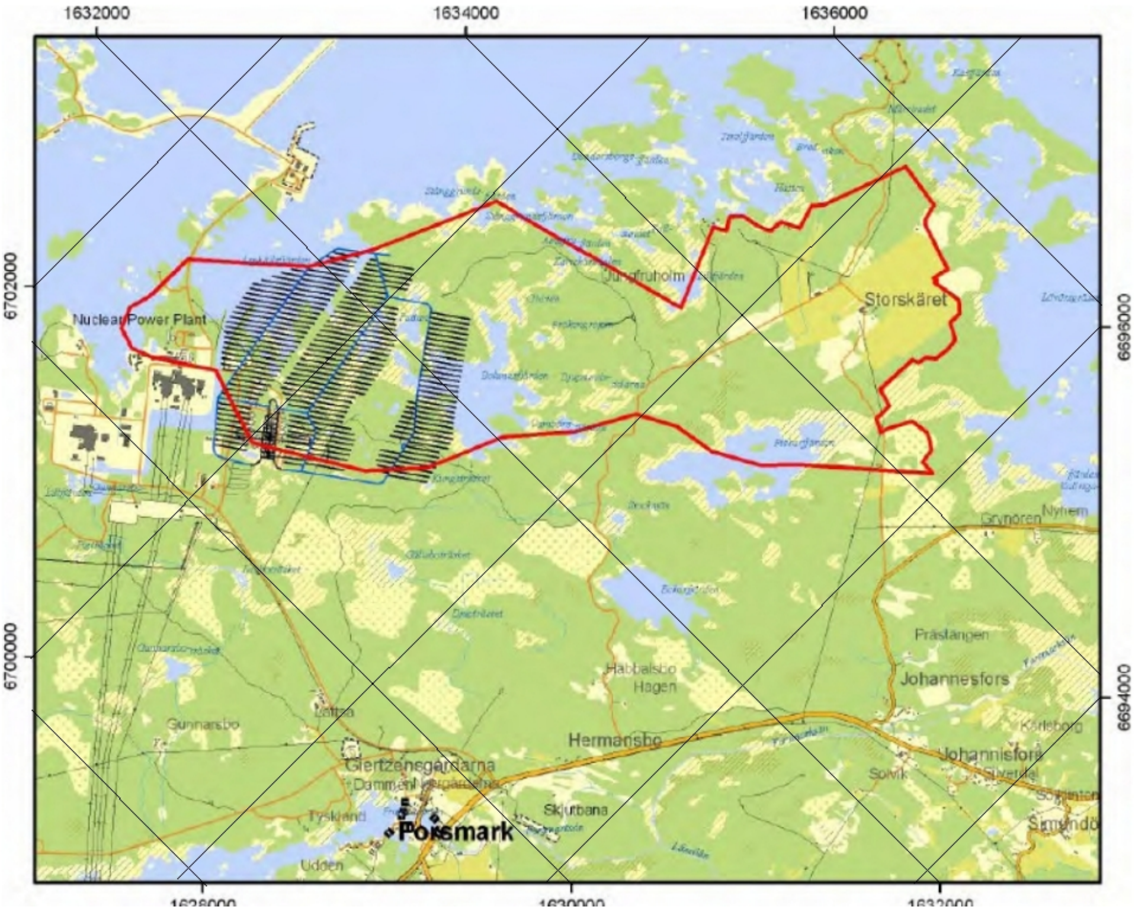

Figure 3.8 *Situation of the D1 repository layout at the Forsmark site (adapted from Brantberger et al. (2006) Figure 5-2 by adding the diagonal grid lines which run North-South and East-West).*

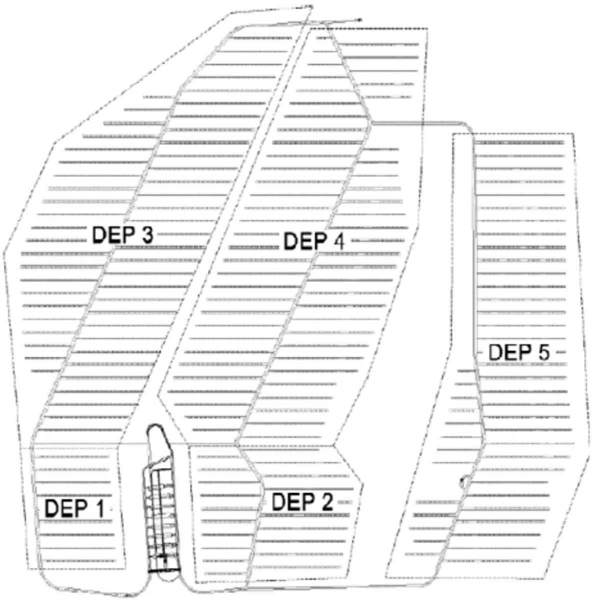

Figure 3.9 *Tunnel layout and construction sequence for Forsmark, based on D1 Design Report Brantberger et al. (2006) Figure 5-9). Note this view is rotated from the reference coordinates (North is approximately 45 degrees to the left from upward in this diagram).*

Figure 3.10 *Tunnel EDZ features and deposition holes for Forsmark repository Section AC (Base Case Realization 01). EDZ features are indicated in yellow; deposition holes for positions that satisfy the deposition-hole criteria in this realization are in green. The grid (grey lines) is a reference grid with 1 km spacing(see caption of Figure 3.7 for explanation).*

Figures 3.10 through 3.12 show the repository layouts for the three sections of the repository. The canister positions vary depending on the realization of the fracture network model, with application of the deposition-hole criteria. Those shown in the figures are for one particular realization of the model.

Figure 3.11 *Tunnel EDZ features and deposition holes for Forsmark repository Section BD (Base Case Realization 01). EDZ features are indicated in yellow; deposition holes for positions that satisfy the deposition-hole criteria in this realization are in green.*

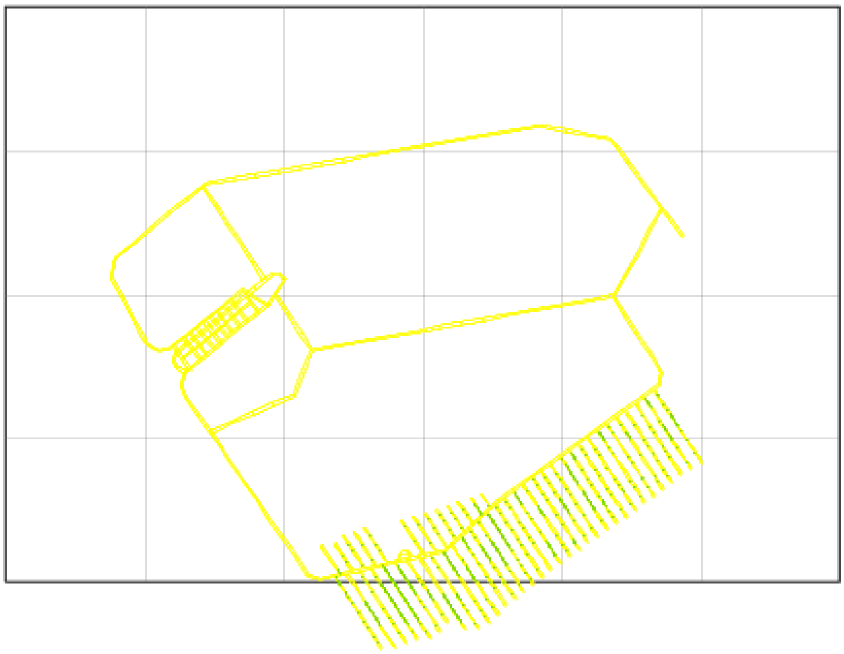

Figure 3.12 *Tunnel EDZ features and deposition holes for Forsmark repository Section E (Base Case Realization 01). EDZ features are indicated in yellow; deposition holes for positions that satisfy the deposition-hole criteria in this realization are in green. The grid (grey lines) is a reference grid with 1 km spacing(see caption of Figure 3.7 for explanation).*

3.3.4 Nested model construction

The DFM model geometry for Forsmark is fully defined by the panel files that describe the components, as described in the foregoing sections. These components are first assembled in a single file which contains all of the geometric features in the model. Figures 3.13 and 3.14 show two views (overview and close-up) of the assembled features for Section AC of the repository.

The assembled features are then converted into a triangular finite-element mesh file using the DFM modules *meshgenx* (with postprocessing script *tripostx*). This resolves all intersections among features (and between features and boundary segments), then triangulates each feature, subject to the constraint that all intersections among features are retained as edges in the mesh. The identities of the original features are retained for each triangular element in the mesh, so that the hydrologic properties of individual features can be modified depending on the realization.

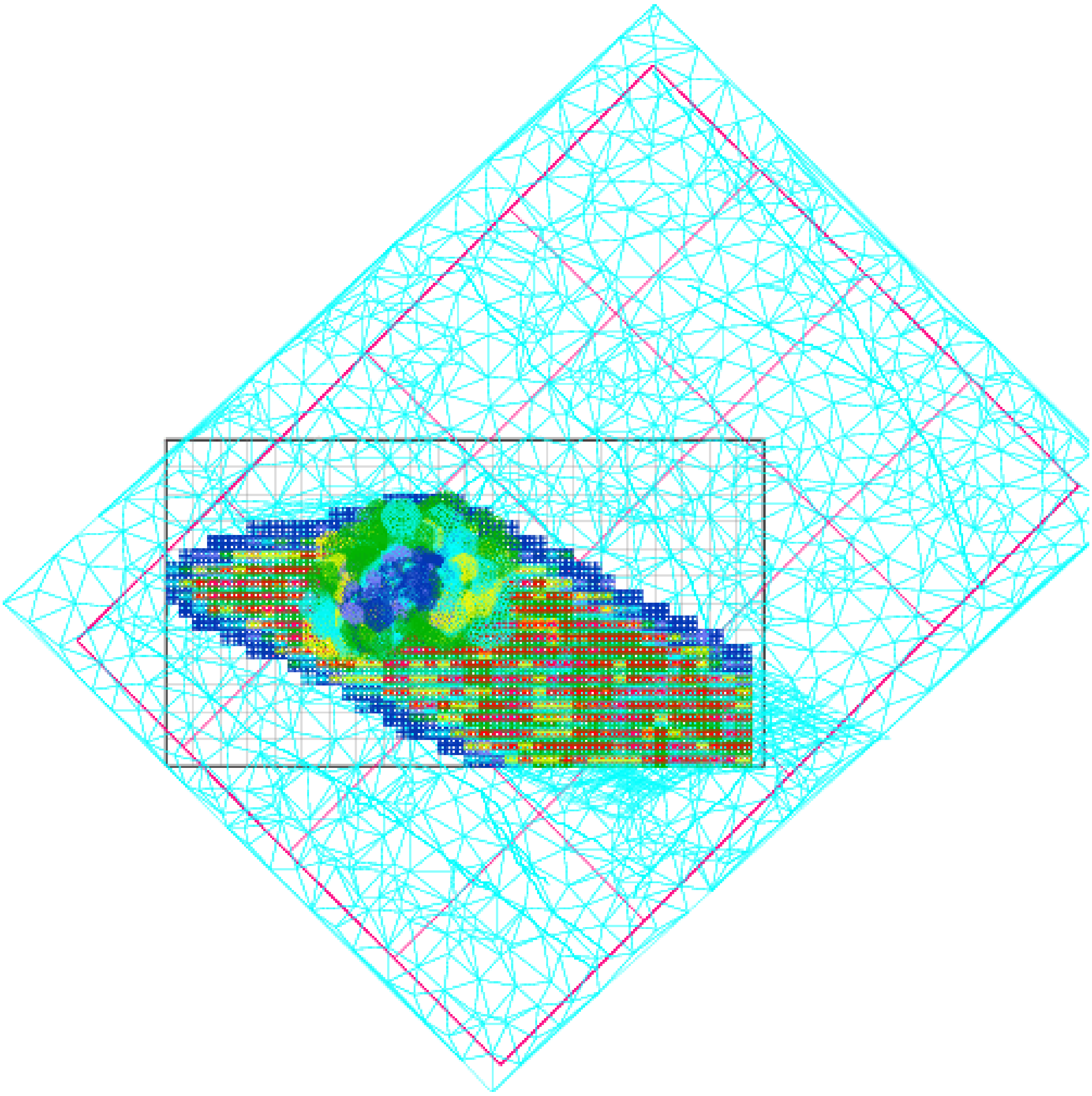

Figure 3.13 *Plan view of combined panels for Forsmark base-case model, Realization 1, Section AC, prior to mesh generation. Colours indicate transmissivity. Note transmissivity values were not assigned to large-scale deformation zones at this point, so these have the same generic value as the topographic feature. The coarse, rectangular grid (magenta) oriented NW-SE and NE-SW indicates panels on the model boundary. The grid (grey lines) is a reference grid with 0.5 km spacing(see caption of Figure 3.7 for explanation).*

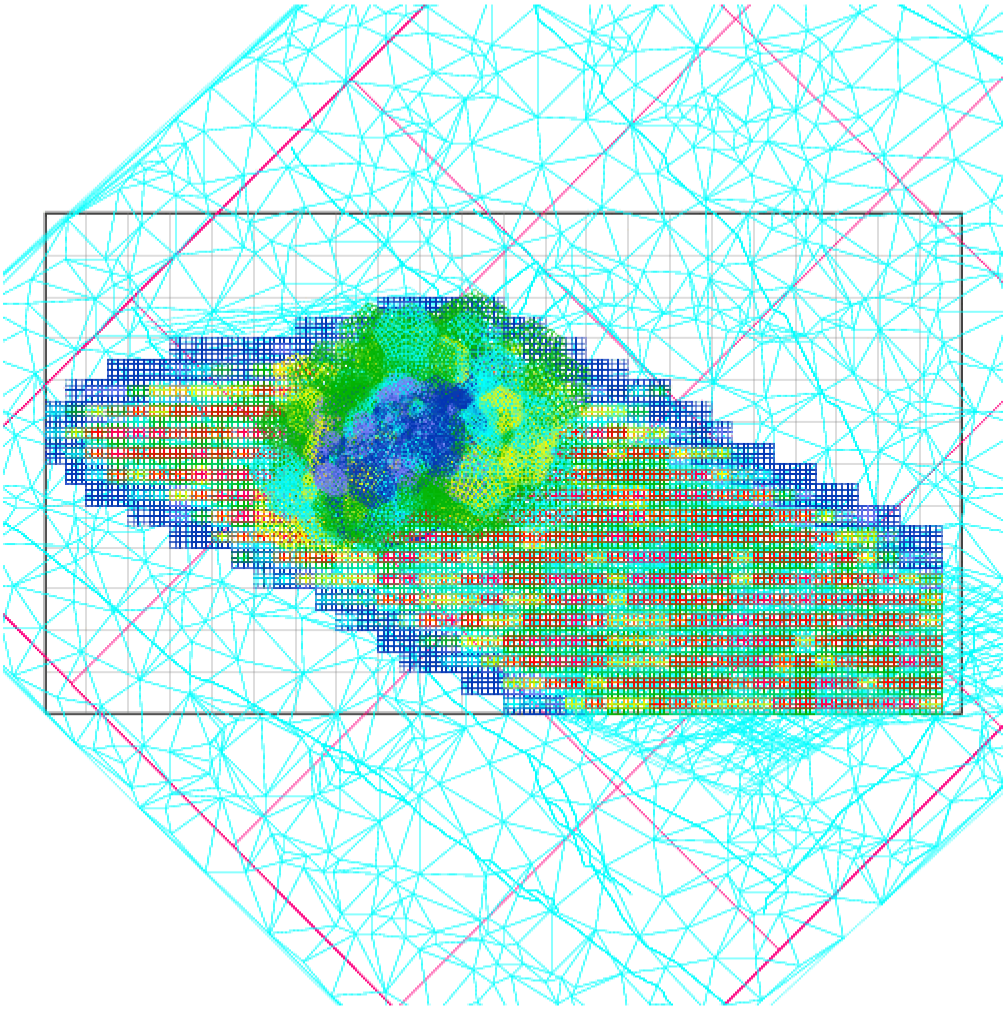

Figure 3.14 *Close-up of plan view of combined panels for Forsmark base-case model, Realization 1, Section AC, to show equivalent grid block resolution around the repository volume. Colours indicate transmissivity. Note transmissivity values were not assigned to large-scale deformation zones at this point, so these have the same generic value as the topographic feature.*

Figure 3.15 shows the mesh that results from performing this procedure on the example shown in Figures 3.13 and 3.14, and after assigning hydrologic properties to the deterministic deformation zones.

Two calculation cases were tested to scope the significance of uncertainty in the hydrologic properties of large-scale (deterministic) deformation zones:

- Uniform DZ transmissivity (Variant *c*): All deformation zones in the deterministic model are assigned a uniform transmissivity of 10^{-5} m^2/s and an effective transport aperture (pore volume per unit area) of 0.2 m, corresponding to a porosity of 0.2 for a 10 m thick zone.

- Base case (Variant *cT*): Deformation zone transmissivities are assigned as best-estimate values based on Table 8-6 of the Forsmark SDM 1.2 report (SKB, 2005); thus different deformation zones may have contrasting properties.

For the base case, in cases where estimates of transmissivity are not available for a particular deformation zone, the depth-dependent formula for gently or steeply-dipping zones given in SKB (2005) Equations 8-7a,b are used (as implemented in the awk-language script FMDZfeatures.awk on the accompanying CD-ROM). Transport aperture and storativity values are calculated according to the empirical formulae given in Equations 8-09 and 8-11 of SKB (2005) as:

$$b[\mathrm{m}] \quad = \quad 0.5 \cdot \sqrt{T[\mathrm{m}^2/\mathrm{s}]}$$

$$S \quad = \quad 7 \cdot 10^{-4} \sqrt{T[\mathrm{m}^2/\mathrm{s}]}$$

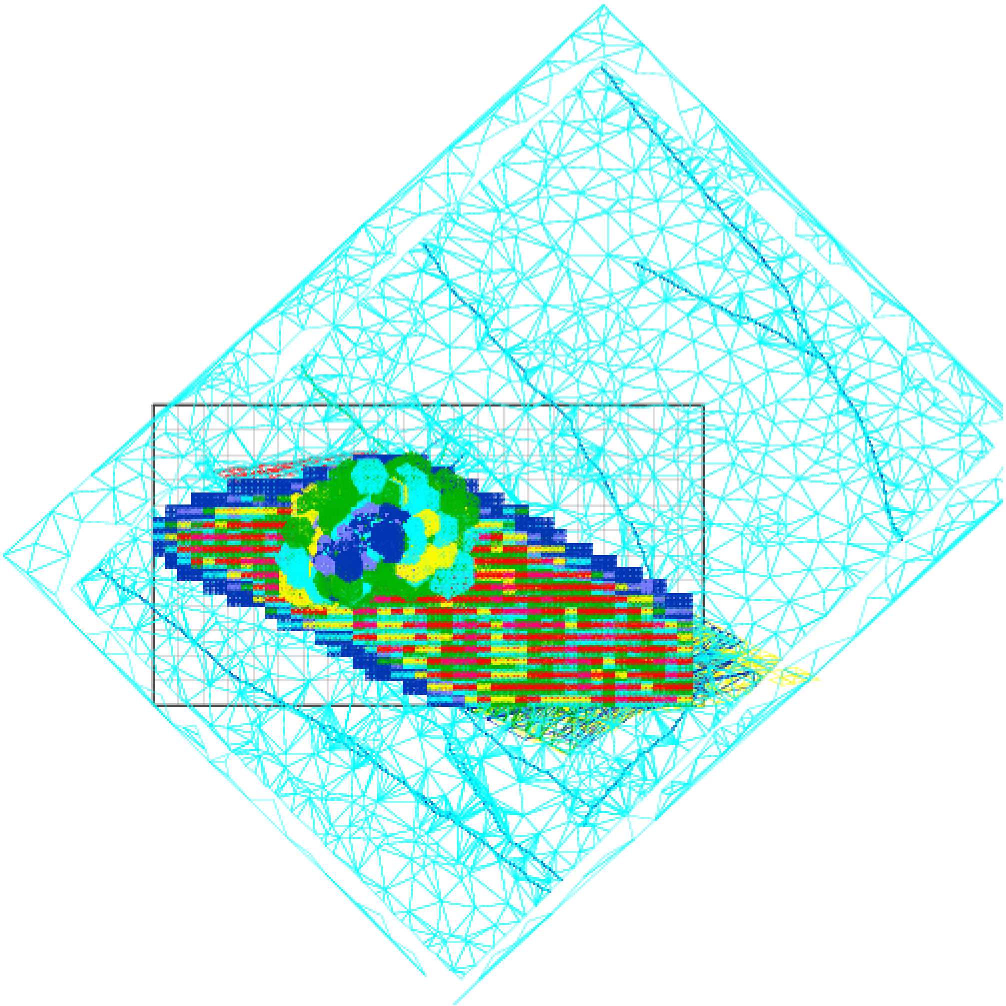

Figure 3.15 *Plan view of mesh (as wireframe) for the AC section of the Forsmark repository (base case model). Colour scale indicates different transmissivity classes. The reference grid (grey lines) is shown for reference.*

3.3.5 Boundary conditions for temperate period

Flow for the temperate period at Forsmark was simulated in response for two different cases.

The base case for the temperate period (Variant *cT*) has a simple topographic gradient, with linearly varying heads along each of the lateral boundaries (based on a fit to the topography along that edge of the model), no-flow conditions at the base, and heads equal to the elevation across the topographic/bathymetric upper surface of the model. This represents a situation of maximum coastline recession, late in an interglacial period (e.g. around 9000 AD, as depicted in Figure 9-13 of SKB, 2006b). This situation represents the maximum head gradient that can be expected across the region of the model, during the ongoing temperate periods or future temperate periods.

A temperate-case variant (Variant *cS*) was used to represent hydrologic boundary conditions similar to those at present. This differs from the base case only in the boundary condition applied to the area of the upper surface that is presently part of the seabed, which is assigned a fixed head equal to zero (since the present-day mean sea level is used as a datum). This approach will somewhat exaggerate the pressure gradients (modelled as equivalent freshwater head gradients) through the model, since in reality the groundwater pressures at the seabed will be higher due to the salinity of the water column.

Table 3.5 *External boundary conditions for Forsmark base case model (cT) and early temperate variant.*

Boundary segment	Type of boundary condition	Value(s)
Southwest side	Specified head	$h = -0.000505\,x + 0.000505\,y + 8.80$ m
Southeast side	Specified head	$h = 0.000806\,x + 0.000806\,y - 2.75$ m
Northeast side	Specified head	$h = 0.000041\,x - 0.000041\,y + 10.24$ m
Northwest side	Specified head	$h = -0.000445\,x - 0.000445\,y + 11.41$ m
Bottom	Specified flux	$q = 0$ (no flow)
Present-day land surface	Specified head	$h = z$
Present-day sea floor	Specified head	$h = z$ (Variant *cT*)
		$h = 0$ (Variant *cS*)

3.4 Variants to scope EBS failure modes

3.4.1 Spalling concepts and state of stress

Spalling around deposition holes can occur when the tangential stresses that result from stress concentrations around the opening exceed the unconfined compressive strength for the rock. Spalling is expected to occur first on the sides of the deposition holes where the tangent to the deposition hole is parallel to the regional maximum compressive stress (typically the direction of maximum horizontal stress, σ_H , and perpendicular to the direction of minimum horizontal stress, σ_h).

When spalling occurs during the period after a deposition hole is bored, the result is a dilation of the deposition-hole wall on the sides where the unconfined compressive strength is exceeded. Sometimes visible slabbing of the rock may occur, in which case this could conceivably be removed so that the bentonite around a canister could swell to fill the gap. However, there could possibly be dilation and fracturing without slabbing, in which case the spalling zone would be more difficult to detect and seal. Hence spalling conditions could lead to transmissive paths, most likely along the sides of the deposition holes which point toward the direction of minimum horizontal stress, σ_h. The possibility that this could lead to enhanced paths for radionuclide transport was explored with variants of the discrete-feature models, as described below.

3.4.2 Basic spalling variant for Forsmark

The basic spalling variant (Variant *cspT*) introduces pathways for flow and transport along the faces of the deposition holes. Spalling is represented in the discrete-feature model by retaining the boundaries of the deposition holes as transmissive features, and triangulating these features along with the other features when the finite-element mesh is produced.

In the basic case, all sides of each deposition hole are assigned transmissivity and aperture values identical with those for the tunnel EDZ features ($T = 5\times10^{-7}$, $b_T = 0.02$ mm).

3.4.3 Directional spalling variant for Forsmark

In the directional spalling case (Variant *cspxT*), the faces of the deposition holes that have normal vectors toward the direction of minimum horizontal stress σ_h (see Figure 3.16) are assigned a higher transmissivity and aperture to represent spalling ($T = 1\times10^{-5}$ m^2/s, $b_T = 1.6$ mm). The direction of σ_h is perpendicular to the maximum horizontal stress σ_H, which has an estimated azimuth of 142° according to the Forsmark Site Descriptive Model v. 1.2 (R-05-18, Table 6-9).

Other faces of the deposition holes are assigned lower transmissivity ($T = 1\times10^{-9}$ m^2/s, $b_T =$ 0.016 mm) to represent a zone of minor damage around deposition holes. The values of transmissivity are arbitrarily chosen due to a lack of data for spalled zones, so this should be viewed simply as a sensitivity study. The transport apertures are calculated from the transmissivity, using the same generic rule that is used for the deformation zones.

These values are applied to the faces of the deposition hole that are below the lower boundary of the tunnel-floor EDZ at -411 m.

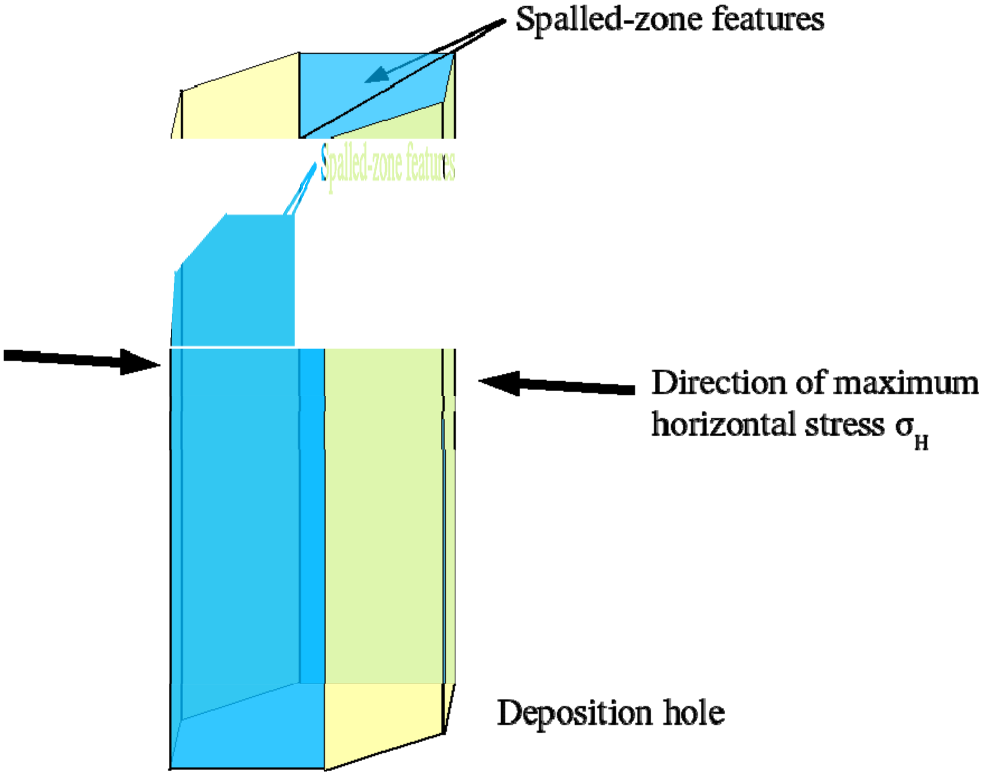

Figure 3.15 Geometry of spalling features for directional spalling variant.

4 Results of calculation cases

4.1 *Laxemar results*

4.1.1 Utilization of deposition tunnels

The utilization factor ε for Laxemar is found to be just over one half (Table 4.1), after accounting for deposition-hole positions that are rejected either because they violate the full-perimeter intersection criterion (FPC) or because the pilot-hole transmissivity exceeds 10^{-5} m^2/s, for the base-case DFN model variant in which transmissivity is semicorrelated to fracture size. Most of the rejected trial positions with this case are due to the FPC criterion; the pilot-hole criterion excludes just 13% of the positions that satisfy the FPC criterion. Presumably this is because, with the semicorrelated DFN model, high-transmissivity fractures tend to be large fractures which are likely to be observed as full-perimeter intersections.

***Table 4.1** Utilization of deposition tunnels for Laxemar DFN model with semicorrelated transmissivity vs. fracture size (single realization). Note that the number of trial positions accepted is based on a minimum center-to-center distance between canisters of 7.8 m; more canisters could be accommodated by using a smaller spacing adapted to the rock type and local thermal properties, as has been done in SKB's design work (Janson et al., 2006).*

Realization	Repository Section	Total tunnel length (m)	Usable length (m)	Trial positions accepted	Utilization	Positions rejected (FPC criterion)	Positions rejected (pilot-hole criterion)
1	A	36950	32834	2394	56.9%	13910	451
1	D	9744	8680	550	49.4%	4363	71
1	E	13316	11664	664	44.4%	6467	52
1	**All**	**60010**	**53178**	**3608**	**53.0%**	**24740**	**574**

4.1.2 Flow for base-case temperate conditions at Laxemar

The distribution of flow magnitudes around deposition holes for the Laxemar base case model is shown in Figure 4.1.

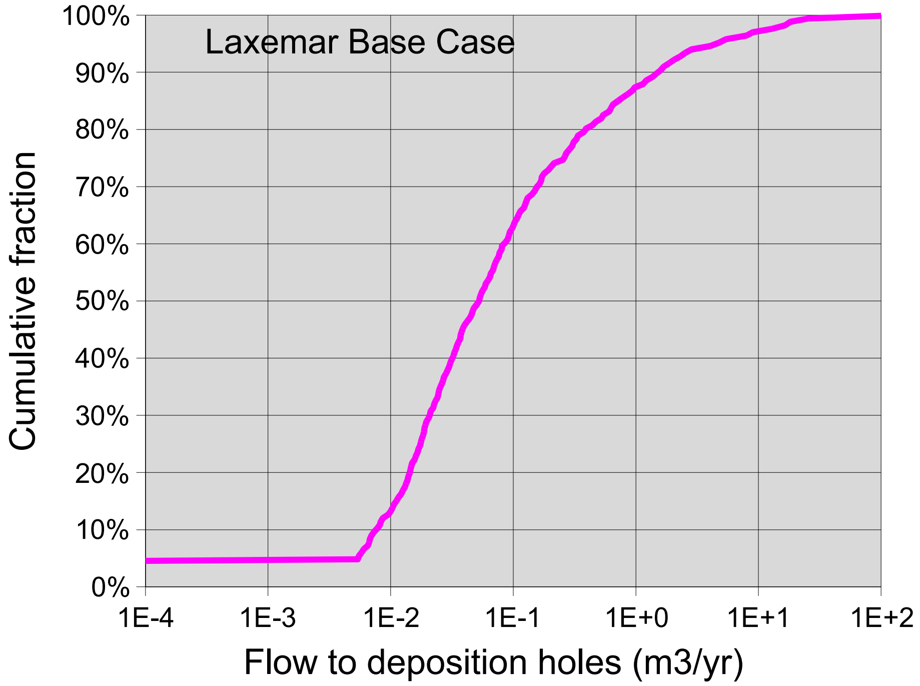

***Figure 4.1** Distribution of flowrates to deposition holes for the Laxemar Base Case model, mid-temperate climate (single realization, Sections D & E only).*

Convergence of the flow solver for this case was inadequate for particle-tracking, due to residual errors in the head solution on the order of one millimetre. However, the solutions are judged to be usable to predict the distribution of flows around deposition holes. For a fracture of transmissivity 10^{-8} m^2/s, a 1 mm error in the head solution could result in errors in the flow on the order of 10^{-4} m^3/yr (*i.e.* at the lower end of the range shown in Figure 4.1).

4.2 Forsmark results

4.2.1 Utilization of deposition tunnels

The utilization factor ε for Forsmark is found to be slightly better than two thirds (Table 4.2), after accounting for deposition-hole positions that are rejected either because they violate the full-perimeter intersection criterion (FPC) or because the pilot-hole transmissivity exceeds 10^{-5} m^2/s, for the base-case DFN model variant in which transmissivity is semicorrelated to fracture size. As for Laxemar, most of the rejected trial positions with this case are due to the FPC criterion, although in this case the pilot-hole criterion excludes 44%

of the positions that satisfy the FPC criterion. Variability in ϵ between DFN realizations appears to be small, with less than a 3% difference between the two realizations that were produced for the Forsmark base-case DFN model.

Table 4.2 *Utilization of deposition tunnels for Forsmark base case DFN model (two realizations). Note that the number of trial positions accepted is based on a minimum center-to-center distance between canisters of 7.8 m; more canisters could be accommodated by using a smaller spacing adapted to the rock type and local thermal properties, as has been done in SKB's design work (Brantberger et al., 2006).*

Realization	Section	Total tunnel length (m)	Usable length (m)	Trial positions accepted	Utilization	Positions rejected (FPI)	Positions rejected (pilot hole)
1	AC	16910.9	15174.9	1383	71.1%	3476	985
1	BD	20076.5	17864.5	1597	69.7%	4013	1508
1	E	11482.4	10194.4	968	74.1%	2116	594
1	**All**	**48469.8**	**43233.8**	**3948**	**71.0%**	**9605**	**3087**
2	AC	16910.9	15174.9	1416	72.8%	3553	643
2	BD	20076.5	17864.5	1427	62.3%	4878	1970
2	E	11482.4	10194.4	943	72.2%	2527	377
2	**All**	**48469.8**	**43233.8**	**3786**	**68.3%**	**10958**	**2990**

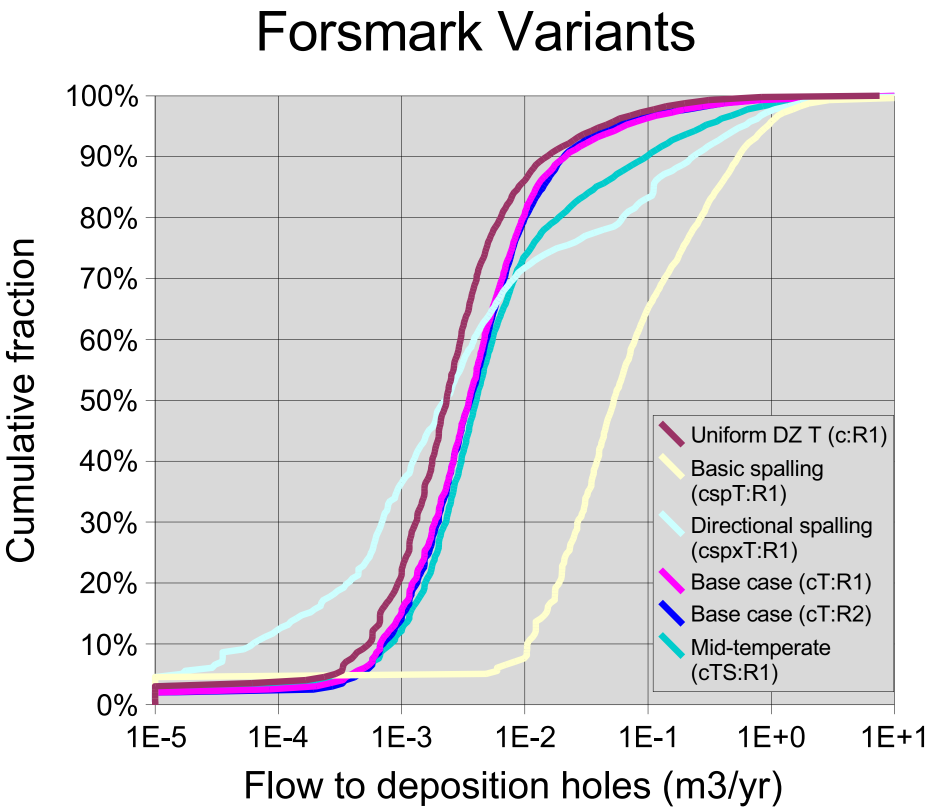

***Figure 4.2** Distribution of flowrates to deposition holes for the Forsmark Base Case model, late temperate climate (Variant cT), present-day temperate climate (Variant cTS), the uniform deformation-zone transmissivity variant (Variant c), and spalling variants (Variants cspT and cspxT). Results are shown for two realizations of the base case (R1 & R2) and for a single realization (R1) of the other variants.*

4.2.2 Flow rates to deposition holes

The distribution in flow rates to deposition holes for Forsmark (Figure 4.2) varies only slightly between realizations of the base-case model. This suggests that the repository covers a sufficiently large volume that ergodicity holds with respect to the stochastic fracture population.

The variant with uniform properties in the large-scale deformation zones (Variant *c*) yields a slight reduction in flow rates to deposition holes, and slightly higher percentage of holes with no significant flow. However, flows for the upper end of the distribution are practically indistinguishable. This appears to support the idea that the hydraulic properties of the large-scale deformation zones, if treated as homogeneous, are not a strong factor in flow to the deposition holes. This might be partly a consequence of the strong role of the EDZ along the tunnel system, for the Forsmark site.

The basic spalling variant (Variant *cspT*) produces roughly an order-of-magnitude increase in flux to the deposition holes. This variant amounts to a uniform EDZ around the deposition holes connecting directly to the deposition tunnels, which presumably acts to enhance flow around each deposition hole.

The directional spalling variant (Variant *cspxT*) yields a more heterogeneous result, with an increase in the flows for the upper end of the flow distribution, but a decrease at the lower end. This is a more heterogeneous model than Variant *cspT*, in which the flow to a given canister depends on whether the nearby fractures link to the high-transmissivity spalling zones, or the low-transmissivity unspalled edges of the deposition holes.

Despite the higher variance, the median flow is close to that for the variants without spalling zones. This is presumably because the zones of elevated transmissivity are localized to opposite sides of each deposition hole, and thus only contribute significantly to flow around the deposition hole if they form links between conductive sub-networks with contrasting heads. The reduced flows to some deposition holes may represent holes that are subjected to lower head gradients, due to short-circuiting of flow through high-transmissivity spalling zones of other holes.

4.2.3 Properties of discharge paths

Statistical measures of the discharge paths for the Forsmark variants, as determined by advective-dispersive particle tracking, are summarized in Tables 4.3 through 4.7 and Figures 4.3 through 4.5. The results presented here are based on mean values for the plume originating from each source (*i.e.*, each deposition-hole).

The EDZ along the tunnels, which is considered to provide a continuous path in these calculations, is a dominant pathway for flow and transport in the very sparse fracture system for Forsmark. Hence many particles released from a given deposition hole end up at neighbouring deposition holes before they reach the surface. In the results presented here, this has been accounted for by convoluting the release path properties from such neighbouring deposition holes, with the properties of the paths between deposition holes.

For most variants, particles were tracked successfully for roughly 80% to 90% of the deposition holes (Table 4.3). Of the remaining fraction of the deposition holes, about 5% represent boreholes with essentially no flow. The remainder are positions where the particle-tracking algorithm either failed due to local imprecision in the head solution, or where particles did not reach a boundary within the maximum allotted simulation time of 10^{10} seconds (about 317 years). This is usually a function of poor local mesh geometry in combination with low gradients, and thus is mainly associated with the positions that have lower flow rates. The directional spalling variant (Variant *cspxT*) has a high proportion of such positions, due to the increased percentage of positions with flow rates of 10^{-4} m^3/yr or less (*i.e.* approaching the effective numerical resolution).

The low number of arrivals for the basic spalling case (Variant *cspT*), despite higher flows around the deposition holes, appears to be due to inadequate convergence of the numerical solution resulting in poor local precision in the head solution. Particle-tracking results for this variant are distinguished from the other variants since they might not be reliably comparable. The directional spalling variant is more realistic and can be considered more reliable.

Table 4.3 *Portion of deposition holes producing arrivals to the surface for the Forsmark temperate variants, including the late-temperate base case (2 realizations), spalling and deformation-zone transmissivity variants, and mid-temperate case. Results for Variant cspT are printed in gray to indicate lower confidence due to numerical problems for this case.*

Variant	Late-temperate (Base Case)		Uniform DZ T	Mid-Temperate	Spalling (directional)	Spalling (basic)
Variant code	*cT*	*cT*	*c*	*cTS*	*cspxT*	*cspT*
Realization No.	1	2	1	1	1	1
Positions tracked	3948	3786	3948	3948	3948	3725
Arrivals	3707	3216	3244	3628	3244	2157
Arrivals	93.9%	85.9%	82.2%	91.9%	76.6%	57.9%

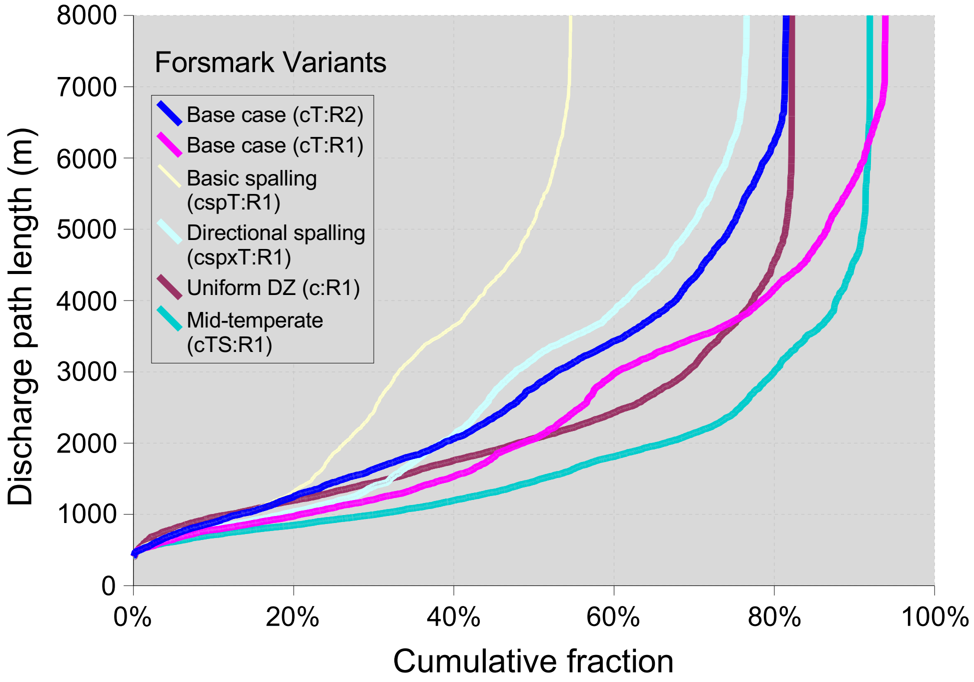

Figure 4.3 *Distribution of discharge-path lengths from deposition holes for the Forsmark Base Case model, late temperate climate (two realizations, Variant cT), uniform deformation-zone variant (Variant c), spalling variants (Variants cspT and cspxT), and mid-temperate climate (Variant cTS). Results are shown for two realizations of the base case (R1 & R2) and for a single realization (R1) of the other variants.*

Discharge-path lengths (Figure 4.3 and Table 4.4) are constrained by the depth to the repository (410 m) and the distance to the edge of the modelled domain, taking into account tortuosity through the discrete-feature network. Median discharge-path lengths are shorter for the mid-temperate variant (*cTS*) where the coastline is at the present-day position, than for the other variants which represent late-temperate conditions when the coastline has receded past the edge of the model domain.

Among the late-temperate variants (excepting Variant *cspT* for which the results are not deemed reliable), the variant with uniform deformation zone properties (Variant *c*) produces shorter discharge-path lengths due to more homogeneous properties in the large-scale network of features. Directional spalling (Variant *cspxT*) produces a minor decrease in the shortest discharge-path lengths which are the paths of greater concern for repository safety, but this effect is only slightly stronger than the difference between realizations of the base-case model (Variant *cT*).

Table 4.4 *Mean transport distances L_r for deposition holes producing arrivals to the surface for the Forsmark late-temperate base case and variants. Results for Variant cspT are printed in gray to indicate lower confidence due to numerical problems for this case.*

Variant	Late-temperate (Base Case)		Uniform DZ T	Mid-Temperate	Spalling (directional)	Spalling (basic)
Variant code	*cT*	*cT*	*c*	*cTS*	*cspxT*	*cspT*
Realization No.	1	2	1	1	1	1
Path length	L_r (m)	L_r (m)	L_r (m)	L_r (m)	L_r (m)	L_r (m)
Mean	2400.17	2517.67	1999.12	1681.75	2480.88	2539.07
Harmonic Mean	1513.69	1660.64	1542.05	1218.58	1505.77	1534.85
Minimum	414.55	411.24	401.55	414.35	413.62	413.62
Percentiles: 1%	514.32	500.43	538.23	509.49	506.09	510.79
10%	777.27	833.14	909.43	703.27	758.54	765.29
25%	1058.67	1270.04	1207.93	898.71	1016.24	1022.10
50%	1926.40	2092.99	1785.76	1340.36	1988.40	2101.89
75%	3491.96	3484.71	2500.30	2097.12	3633.75	3728.47
90%	4662.61	4819.05	3568.03	3347.95	4927.22	4913.85
99%	6643.48	6419.69	4973.69	4943.33	6658.28	6692.81
Maximum	9270.74	7967.64	6586.47	6826.85	8888.10	9231.40

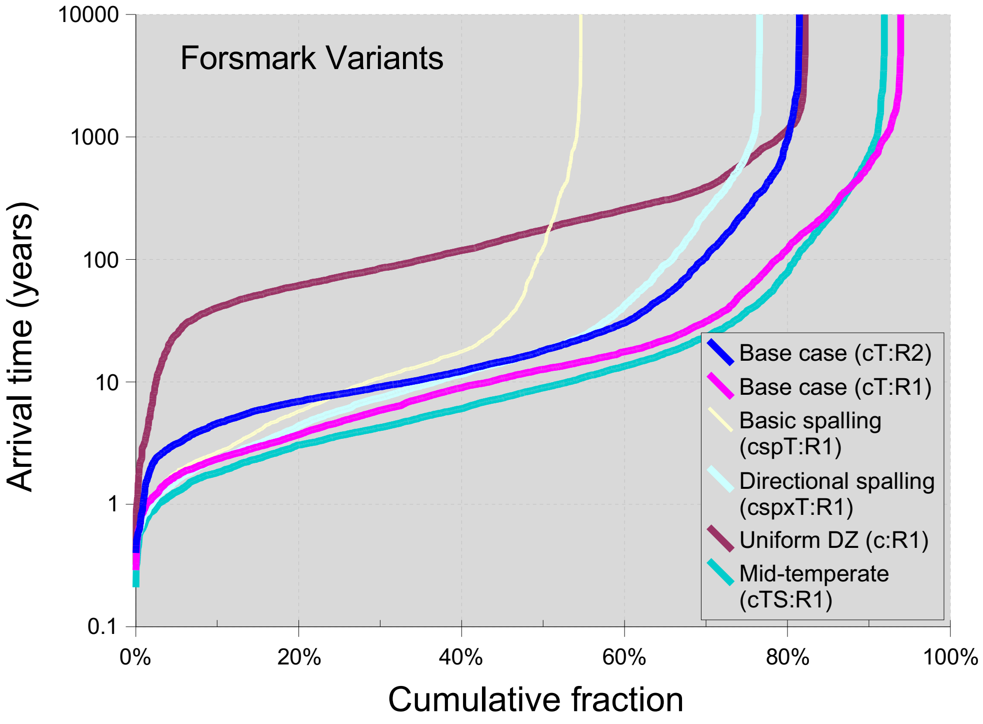

Figure 4.4 *Distribution of travel times for discharge from deposition holes to the surface, for the Forsmark Base Case model, late temperate climate (two realizations, Variant cT), uniform deformation-zone variant (Variant c), spalling variants (Variants cspT and cspxT), and mid-temperate climate (Variant cTS). Results are shown for two realizations of the base case (R1 & R2) and for a single realization (R1) of the other variants.*

Travel times for advective-dispersive transport (not accounting for sorption or matrix diffusion) from deposition holes to the surface are presented in Figure 4.4 and Table 4.5. Median transport times are only slightly shorter for the mid-temperate variant (Variant *cTS*) compared to the base-case variant which represents late-temperate conditions when the coastline has receded.

Among the late-temperate variants (excepting Variant *cspT* for which the results are not deemed reliable), the variant with uniform deformation zone properties (Variant *c*) produces an order of magnitude slower transport relative to the base case. This is presumably because the homogeneous properties in the large-scale features reduce the possibilities for fast paths from the repository to the surface. Directional spalling (Variant *cspxT*) produces a slight decrease in arrival times for the faster paths, which is comparable in magnitude to the difference between realizations of the base-case model (Variant *cT*).

Table 4.5 *Mean transport times t_r for deposition holes producing arrivals to the surface for the Forsmark late-temperate base case and variants. Results for Variant cspT are printed in gray to indicate lower confidence due to numerical problems for this case.*

Variant	Late-temperate (Base Case)		Uniform DZ T	Mid-Temperate	Spalling (directional)	Spalling (basic)
Variant code	*cT*	*cT*	*c*	*cTS*	*cspxT*	*cspT*
Realization No.	1	2	1	1	1	1
Path length	t_r (yr)	t_r (yr)	t_r (yr)	t_r (yr)	t_r (yr)	t_r (yr)
Mean	94.1	90.8	236.7	68.5	75.9	60.3
Harmonic Mean	5.7	8.5	44.5	4.2	5.1	4.7
Minimum	0.3	0.4	0.3	0.2	0.3	0.3
Percentiles: 1%	0.9	1.0	2.9	0.7	0.7	0.8
10%	2.3	4.2	36.1	1.8	2.0	1.9
25%	4.4	7.3	62.3	3.3	4.1	3.5
50%	11.5	13.0	122.3	7.7	10.8	9.4
75%	32.1	33.8	270.9	22.0	30.8	18.8
90%	226.3	192.1	569.8	139.8	194.6	94.5
99%	1426.8	1451.0	1516.2	1013.2	986.9	984.5
Maximum	4671.7	7938.5	4600.8	4671.7	4983.0	4543.8

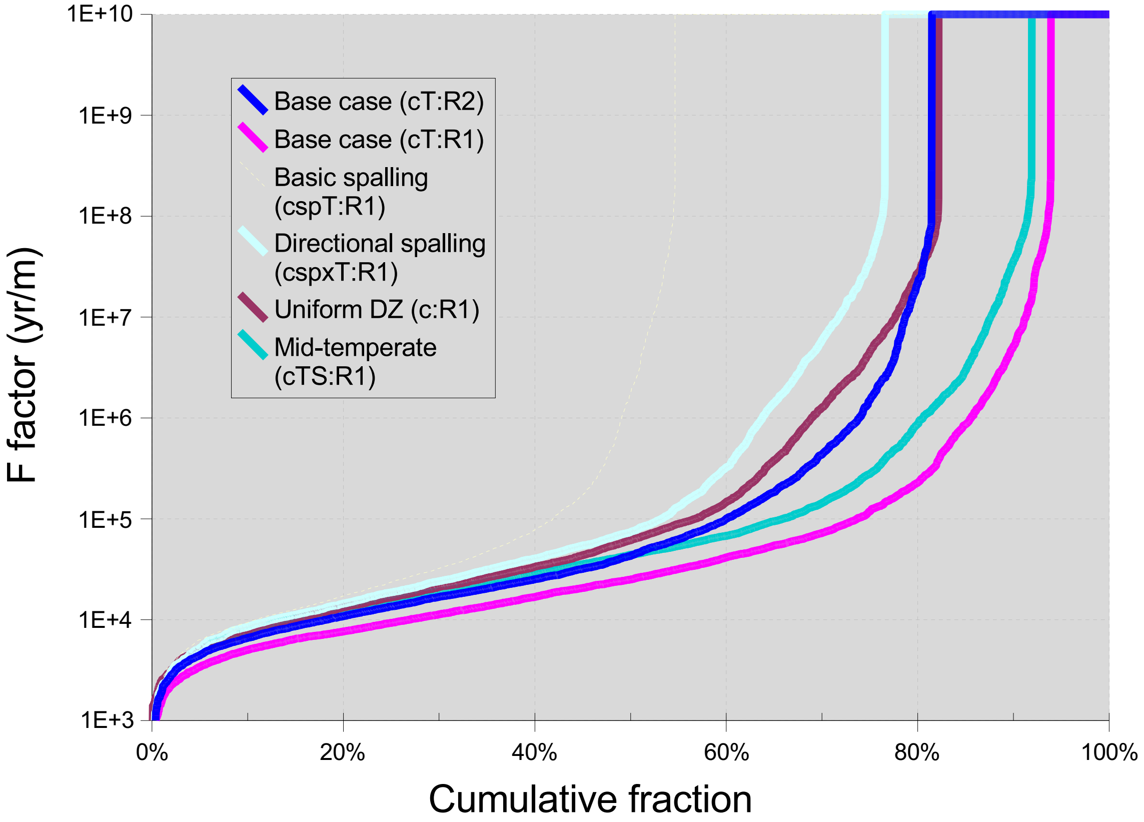

Figure 4.5 *Distribution of F for discharge paths from deposition holes to the surface, for the Forsmark Base Case model, late temperate climate (two realizations, Variant cT), uniform deformation-zone variant (Variant c), spalling variants (Variants cspT and cspxT), and mid-temperate climate (Variant cTS). Results are shown for two realizations of the base case (R1 & R2) and for a single realization (R1) of the other variants.*

Transport resistances F_r for the ensemble of deposition-hole positions are presented in Figure 4.5 and Table 4.6. Median transport resistances are slightly higher for the mid-temperate variant (Variant *cTS*), despite the slightly shorter median discharge-path lengths and slightly faster median arrivals to the surface, when the coastline is near the repository as at present. This result (although less than the differences between realizations of the base case) seems counterintuitive. It implies that particles encounter more wetted surface per unit volume of water along the release paths in the mid-temperate case, which means that transport apertures are smaller over the most critical parts of the release paths. This result is likely sensitive to assumptions about the relationship between transport aperture and transmissivity in the central portion of the model.

Among the late-temperate variants (excepting Variant *cspT* for which the results are not deemed reliable), the variant with uniform deformation zone properties (Variant *c*) shows only minor differences in transport resistance, relative to the base case. Thus the shorter transport paths in the more homogeneous large-scale network are compensated for by slower transport times.

Differences between realizations of the base-case model (Variant *cT*) are minor over most of the range of F_r, in terms of statistics for deposition holes that produce releases to the surface. The main difference seen in the overall distribution (Figure 4.5) is due to variation in the percentage of deposition holes that produce releases, which reflects chance intersections with the the stochastic features (single fractures or minor deformation zones).

Directional spalling (Variant *cspxT*) produces a moderate increase in F_r , perhaps due to the additional porosity and wetted surface close to the source. The sensitivity of this result to the hydraulic parameters of the spalled zones (which were arbitrarily chosen) has not been investigated; this could be significant for the results.

Table 4.6 *Mean transport resistance F_r for deposition holes producing arrivals to the surface for the Forsmark late-temperate base case and variants. Results for Variant cspT are printed in gray to indicate lower confidence due to numerical problems for this case.*

Variant	Late-temperate (Base Case)		Uniform DZ T	Mid-Temperate	Spalling (directional)	Spalling (basic)
Variant code	*cT*	*cT*	*c*	*cTS*	*cspxT*	*cspT*
Realization No.	1	2	1	1	1	1
Transport resistance	F_r (yr/m)	F_r (yr/m)	F_r (yr/m)	F_r (yr/m)	F_r (yr/m)	F_r (yr/m)
Mean	1.56×10^6	1.40×10^6	2.27×10^6	2.45×10^6	2.79×10^6	2.02×10^6
Harmonic Mean	1.05×10^4	1.30×10^4	1.68×10^4	1.38×10^4	1.49×10^4	1.34×10^4
Minimum	8.26×10^1	1.00×10^2	7.23×10^2	4.30×10^1	8.26×10^1	1.23×10^2
Percentiles: 1%	1.49×10^3	1.77×10^3	2.26×10^3	1.77×10^3	1.92×10^3	1.87×10^3
10%	4.83×10^3	5.84×10^3	6.52×10^3	7.21×10^3	7.16×10^3	6.56×10^3
25%	8.77×10^3	1.11×10^4	1.37×10^4	1.44×10^4	1.38×10^4	1.18×10^4
50%	2.24×10^4	2.64×10^4	3.51×10^4	3.69×10^4	3.72×10^4	2.72×10^4
75%	7.50×10^4	1.19×10^5	1.89×10^5	1.30×10^5	1.88×10^5	8.76×10^4
90%	7.72×10^5	9.02×10^5	3.10×10^6	1.66×10^6	4.24×10^6	1.07×10^6
99%	4.41×10^7	3.78×10^7	4.98×10^7	6.21×10^7	6.39×10^7	5.62×10^7
Maximum	2.28×10^8	2.80×10^8	1.46×10^8	2.29×10^8	2.01×10^8	2.02×10^8

4.2.4 Release points to the near-surface environment

Particles in the discrete-feature model are tracked until they reach a boundary of the model, most often the topographic surface (if on land) or bathymetric surface (if to the sea bed). Such particles are considered to have arrived at the geosphere-biosphere interface. The locations at which the particles arrive at this interface are plotted in Figures 4.7 through 4.11. Note that the discrete-feature model uses a very simplified representation of the near-surface bedrock, Quaternary cover and surficial waters, so more detailed models of the shallow system would be needed to predict paths for transport in those parts of the system.

For the late-temperate base case model (Figure 4.7), discharge primarily is along a gently-dipping, NNE-striking structure (ZFMNE00B7 in SKB's nomenclature) that outcrops under Asphällsfjärden, and secondarily along a gently-dipping, ENE-striking structure (ZFMNE00A2) that outcrops under the Baltic further east. A few particles emerge in other gently- to steeply dipping, NE-striking deformation zones near where these connect to the steeply dipping Singö Zone (ZFMNW001); particles emerging at these locations generally have longer travel times. The fastest particles to reach the surface mainly originate from sources in the part of the repository that lies west of ZFMNE00B7 in plan view, as indicated by the pattern of tiny red dots in Figure 4.6.

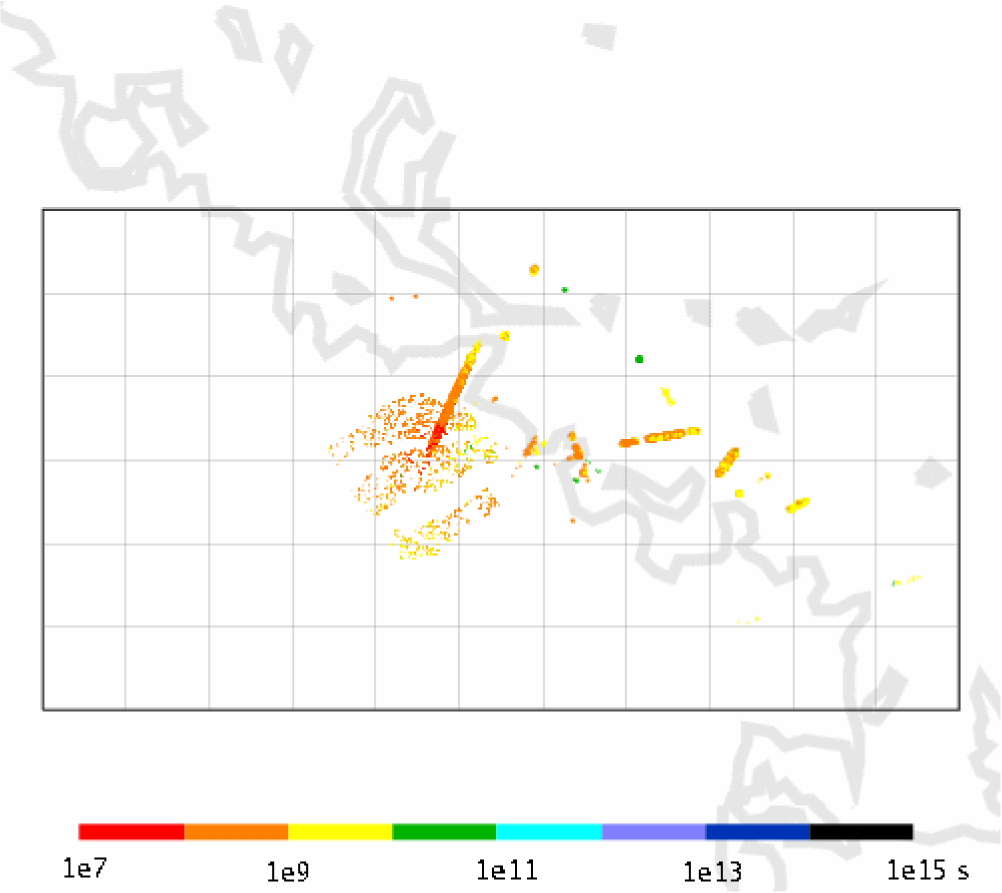

Figure 4.6 *Arrivals for Forsmark late-temperate base case (Variant cT), Realization 01. Plan view showing source canister locations (tiny dots) and arrival locations (larger squares) for particles that reach the surface, with colour indicating age of particle when it reaches the surface (logarithmic scale from* 10^7 *to* 10^{15} *seconds, corresponding approximately to 0.3 to* 3×10^7 *years).*

The second realization of the late-temperate base-case model (Figure 4.7) produces a similar pattern of arrivals, except that another gently-dipping, NNE trending deformation zone (ZFMNE00B6) produces a band of arrivals directly north of the easternmost section of the repository, and the number of fast paths from this section is increased while the number of fast paths from the other sections via ZFMNE00B7 is reduced. Thus it appears that the uncertainty represented in the stochastic fracture network can account for significant shifts in the locus of discharge, and in terms of which parts of the repository give worst performance. This may be significant for SKB's design approach during the construction phase, as it implies that optimization of the layout will still require reduction in uncertainty regarding the discrete-fracture population.

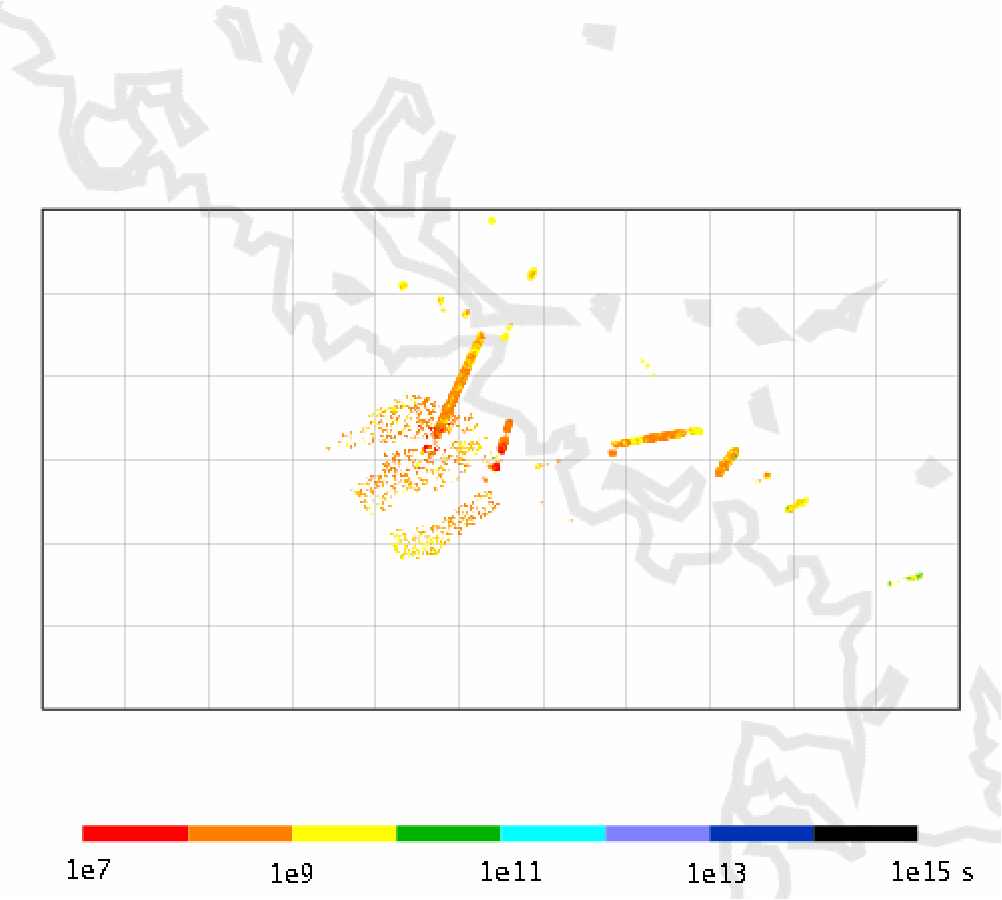

Figure 4.7 *Arrivals for Forsmark late-temperate base case (Variant cT), Realization 02. Plan view showing source canister locations (tiny dots) and arrival locations (larger squares) for particles that reach the surface, with colour indicating age of particle when it reaches the surface (logarithmic scale from* 10^7 *to* 10^{15} *seconds, corresponding approximately to 0.3 to* 3×10^7 *years).*

The pattern of discharge for the late-temperate case with uniform transmissivity values in all large-scale deformation zones (Figure 4.8) yields a more diffuse pattern of discharge, with particles discharging through nearly all of the structures that outcrop NE of the repository. Travel times are slower overall in this calculation case, but as with the base case, the northwestern part of the repository produces generally faster arrivals.

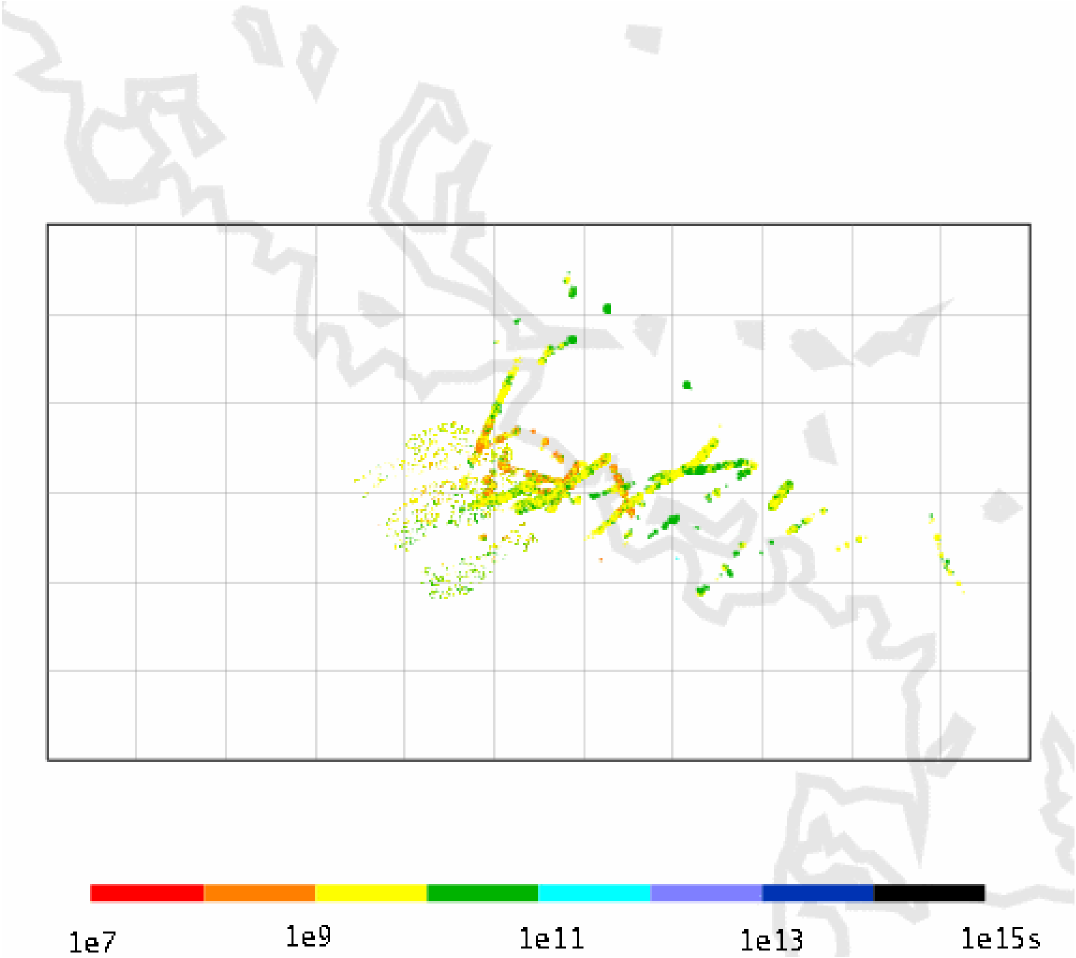

Figure 4.8 *Arrivals to surface for Forsmark Uniform deformation-zone transmissivity variant, Realization 01. Plan view showing source canister locations (tiny dots) and arrival locations (larger squares) for particles that reach the surface, with colour indicating age of particle when it reaches the surface (logarithmic scale from* 10^7 *to* 10^{15} *seconds, corresponding approximately to 0.3 to* $3x10^7$ *years).*

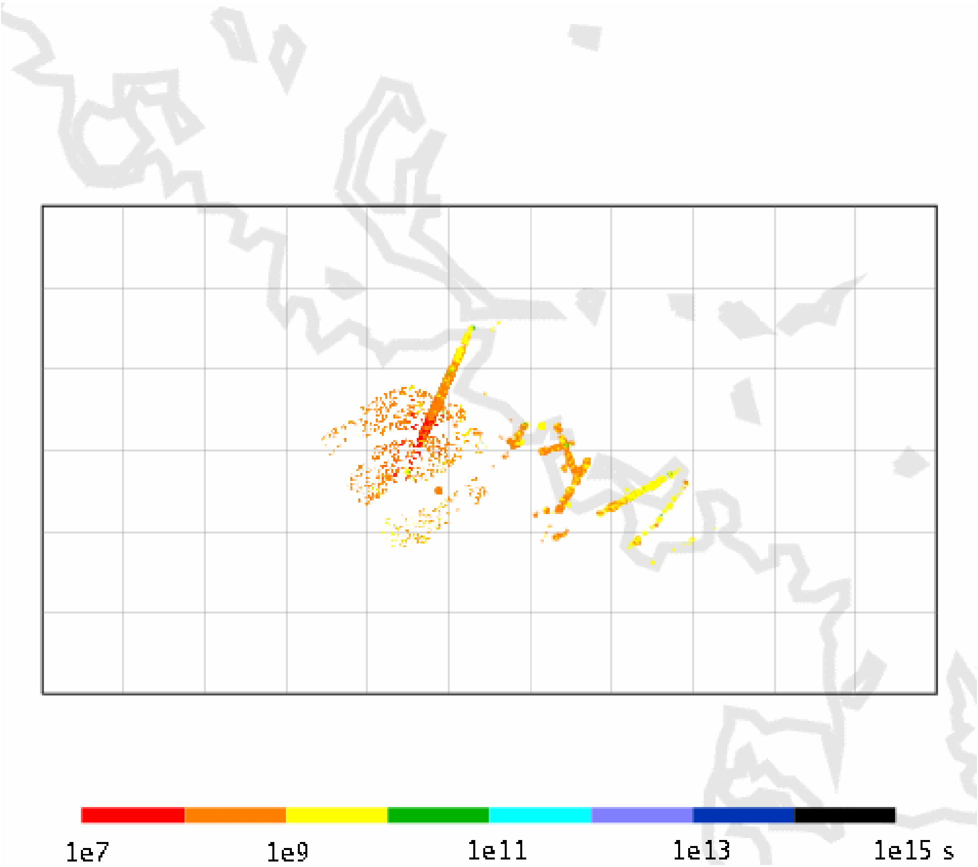

Figure 4.9 *Arrivals to surface for Forsmark mid-temperate case (Variant cTS), Realization 01. Plan view showing source canister locations (tiny dots) and arrival locations (larger squares) for particles that reach the surface, with colour indicating age of particle when it reaches the surface (logarithmic scale from* 10^7 *to* 10^{15} *seconds, corresponding approximately to 0.3 to* $3x10^7$ *years).*

The mid-temperate case with the coastline at the present-day location (Figure 4.9) produces a pattern of discharge that is more compressed in the NE-SW direction. Due to the uniform-head boundary condition under the seabed, discharge is essentially confined by the modern shoreline, and no particles reach the Singö Zone. Instead, structures to the east of the repository discharge in the Dundersborgsfjärden area. By comparison with the late-temperate cases, this indicates that discharge areas will shift progressively NE during interglacial periods, but may ultimately be limited by the Singö Zone.

When spalled zones are included around the deposition holes (Figures 4.10 and 4.11), the patterns of discharge to the surface are nearly identical with the base case model for the same realization. Thus spalling around deposition holes appears to have a negligible effect on the large-scale pattern of discharge, although it can influence travel times and transport resistances for the transport paths that are essentially the same in both cases.

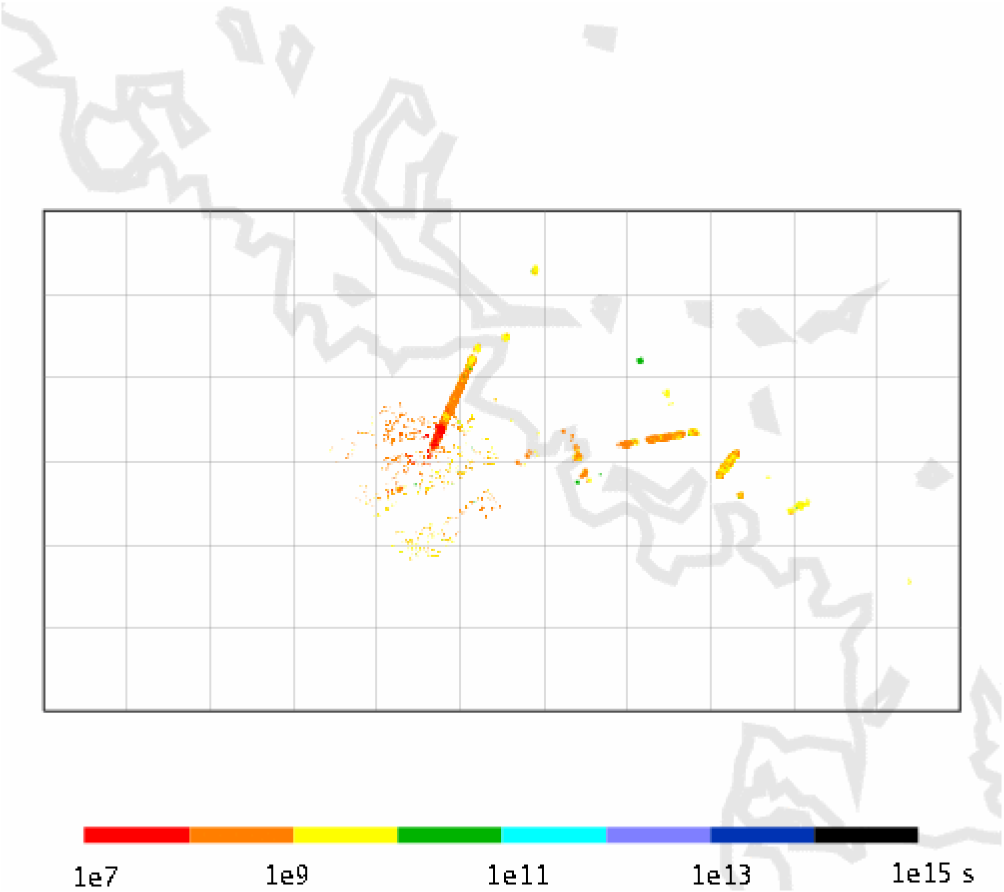

Figure 4.10 *Arrivals to surface for Forsmark spalling variant (basic), Realization 1. Plan view showing source canister locations (tiny dots) and arrival locations (larger squares) for particles that reach the surface, with colour indicating age of particle when it reaches the surface (logarithmic scale from* 10^7 *to* 10^{15} *seconds, corresponding approximately to 0.3 to* $3x10^7$ *years).*

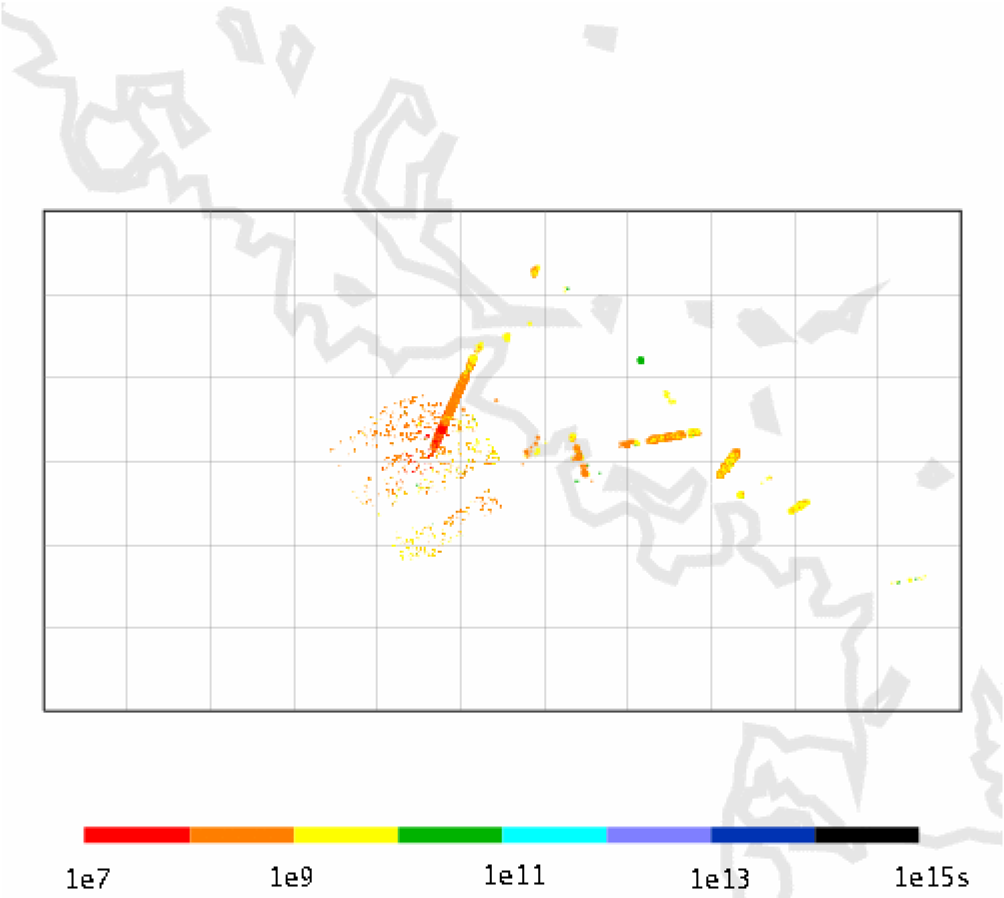

Figure 4.11 *Arrivals to surface for Forsmark late-temperate case with directional spalling (Variant cspx), Realization 01. Plan view showing source canister locations (tiny dots) and arrival locations (larger squares) for particles that reach the surface, with colour indicating age of particle when it reaches the surface (logarithmic scale from* 10^7 *to* 10^{15} *seconds, corresponding approximately to 0.3 to* $3x10^7$ *years).*

5 Discussion of results

5.1 Utilization factors

The calculated utilization factors $\varepsilon = 0.68$ to 0.71 for the full repository at Forsmark and $\varepsilon = 0.53$ for the full repository at Laxemar are significantly lower than the corresponding values $\varepsilon = 0.93$ and $\varepsilon = 0.88$ for the most nearly comparable cases presented in Table 9-6 of the SR-Can Main Report (SKB, 2006b). The reasons for this discrepancy need to be explored.

SKB's calculation was based on an analytical model which has not yet been fully presented, but apparently is based on an earlier derivation (Hedin, 2005) which relates the frequency of full-perimeter fracture intersections with tunnels to the percentage of canisters that are rejected. This might not be conservative since a single FPC fracture that is subparallel to the deposition tunnel can result in the exclusion of more than one canister position. The analytical model also takes credit for a zone of smaller seismic displacement near the edges of the assumed, disc-shaped fractures. This is justified by analytical models for idealized, isolated fractures, but is nonconservative for joint systems in which fractures terminate against other fractures (as is commonly observed in granitic sites) so that edges of fractures do not necessary act as zero-displacement boundaries.

The simulation approach used here checks explicitly for intersections between FPC fractures and canister positions, so it accounts for the possibility that a single FPC fracture can result in exclusion of multiple deposition hole positions. It also does not take credit for reduced displacements near fracture edges. However, as noted by Hedin (2005), a simulation approach can be overly conservative when used with finite generation domains, especially in conjunction with a power-law models for fracture size (as is the case here). Further investigation with sensitivity studies is needed to determine the degree to which the much lower values of ϵ obtained in this study are attributable to such effects.

5.2 Flow around deposition holes

The distribution of flow to deposition holes is an important factor for longevity of the engineered barriers (buffer and canister) as well as for fuel dissolution and transport away from the deposition holes in the event that these barriers fail.

Results for the set of Forsmark variants presented here suggest that the distribution of flow to deposition holes is not sensitive to the particular realization of the stochastic discrete-fracture population (DFN submodel). This presumably means that the number of canister positions and the volume of rock modelled around the repository are large enough to encompass the stochastic variability expressed in the DFN submodel.The variants completed thus far do not include alternative conceptual models (such as DFN submodels with increased clustering of fractures or hierarchical structure), or variants with respect to key properties of the DFN submodel, such as the assumed correlation of size to transmissivity.

The flow distribution to deposition holes is not very sensitive to the hydrologic properties of the large-scale deformation zones. The DFN submodel, the EDZ around tunnels, and spalled zones in the deposition-hole walls (if present), appear to be the main controls on this distribution. This result could be expected, as it reflects that in a heterogeneous discrete system, local flows are dominated by the properties of local features, provided that a well-connected, percolating network exists on larger scales.

The results in terms of flow rate distribution appear to be only moderately sensitive to coastline recession as the temperate period proceeds. Flow rates during periods of glacial retreat could be much higher, by an order of magnitude or more. The relatively small variability in flow rates over the mid- to late-temperate period might not need to be considered in calculations of engineered barrier degradation.

5.3 Transport paths to the biosphere

A very important feature of the models presented here is the presence of transmissive features representing a continuous excavation-damaged zone (EDZ) and/or backfill gaps along all tunnels. For Forsmark in particular, this is significant transport feature due to the apparent sparseness of the fracture population. If a continuous EDZ can be avoided out by use of full-face tunnel-boring machines or by carefully controlled drill-and-blast methods for excavating drifts (as has been suggested based on one experiment in the Äspö Hard Rock Laboratory), if roof spalling due to stress conditions can be avoided by careful tunnel design, and if backfill gaps after settling can be avoided, then these models might be overly conservative in this respect. However, the possibility to avoid these conditions has not yet been conclusively demonstrated. The importance of the continuous EDZ could be tested in the discrete-feature model by means of variants in which EDZ transmissivity is reduced to very low values for parts of the tunnels.

Another important feature of the models is that they represent an entirely freshwater system. Both Laxemar and Forsmark are situated at the coast where brackish Baltic water has a higher density than near-surface groundwater and meteoric water, and very dense brines (of disputed origin, either relict or a consequence of rock-water interaction) may be present at depth. From models that take density-dependent flow and coupled diffusion of dissolved salts into account (including the models used by SKB for SR-Can predictions), it is expected that this situation will decrease both the depth of groundwater circulation cells and the fluxes at repository depth, for the present-day situation.

Hence the freshwater models used in this study likely exaggerate the flows and groundwater velocities. This may in large part account for the higher values of flow and reduced values of travel time and transport resistance, relative to SKB's modes. This is most important for simulations of early- to mid-temperate stages, and presumably be less important for the late-temperate case where the freshwater/seawater interface has moved seaward, and for the glacial retreat case where a high volume of glacial meltwaters and very high head gradients may effectively flush the system.

Considering these limitations of the models and what has been considered, the cases presented here might best be viewed as representing the relative effects of different features and properties.

For consequence calculations for transport of radionuclides from a repository, the most important single measure of transport paths is the transport resistance, F_r. Other pathway parameters presented here (L_r and t_r) are primarily useful for understanding how the observed effects on F_r might arise from a given variant of the model. The most critical part of the F_r distribution is the low end; radionuclide retention in the geosphere for repository time scales can be very sensitive to low values of F_r, but retention effectively becomes infinite for higher values.

For the Forsmark model variants considered here, the lower end of the F_r distribution (Figure 4.5) is not strongly sensitive to the attributes that have been changed. Spalling around deposition holes yields a slight increase in F_r (less than a factor of two). This result is likely sensitive to the assumptions regarding hydraulic properties of the spalled zones, which have been arbitrarily specified for lack of relevant data. Further investigation of the sensitivity of the F_r distribution to assumptions regarding these parameters is warranted.

Although the distribution of flows to deposition holes was found to be insensitive to stochastic realizations of the DFN submodel, the lower end of the F_r distribution does show a sensitivity to stochastic variation which could be significant for consequence calculations. Given that many uncertainties in the DFN submodel have not been resolved, including major conceptual uncertainties (*e.g.* clustering or hierarchical structure), further exploration of these uncertainties is needed.

The lower end of the F_r distribution is not strongly dependent on the stage of temperate climate, at least between the two cases (mid- and late-temperate) that have been considered here. The present-day (mid-temperate) situation is the more pessimistic case due to the relatively short discharge-path lengths caused by proximity to the sea. However the difference is seen mainly for the (less critical) upper part of the F_r distribution, since the main effect is to confine the longer discharge paths. As seen from the plots of discharge locations (Figures 4.6 and 4.9), under present-day conditions the longer paths that discharge via the Singö Zone are eliminated.

Plots of source and discharge location (Figures 4.6 through 4.11) show that stochastic variability in the DFN submodel, variability in large-scale deformation zone properties and future climate states can all influence which parts of the repository produce the fastest arrivals, and where these arrive in the biosphere. The first means that optimization of the repository layout with respect to performance will be not be possible until further information is available from the construction phase to reduce these uncertainties (if in fact they are significantly reducible). The second means that the locus of discharge is likely to shift with coastal recession and possibly with reactivation of fractures and fracture zones caused by long-term climate change.

None of the model variants in the present study have included large-scale heterogeneity within deformation zones. Existence of such heterogeneity is supported by the observed variability in local hydraulic properties between different borehole intersections with deformation zones. However, an understanding of correlation scales within deformation zones is lacking. Models that incorporate large-scale, spatially correlated properties within deformation zones will exhibit greater large-scale heterogeneity, with more chance for extreme, low F_r pathways (Tsang et al., 1996; Geier, 1996). While such models are notoriously difficult to parametrize based on borehole data alone, studies of deformation-zone structure from surface exposures (Geier, 2005) may be helpful for formulating plausible spatial correlation models; additional information of relevance can be expected from SKB's ongoing minor deformation zone (MDZ) study at Laxemar.

6 Conclusions

Utilization factors

The utilization factors of $\varepsilon = 0.70$ obtained here for the full repository at Forsmark and $\varepsilon = 0.53$ for the full repository at Laxemar are significantly lower than the corresponding values $\varepsilon = 0.93$ and $\varepsilon = 0.88$ for the most nearly comparable case presented in Table 9-6 of the SR-Can Main Report (SKB, 2006b). Further investigation is needed to discern whether this discrepancy is primarily due to possible nonconservative assumptions in SKB's analytical modelling approach, or due to artefacts of the simulation approach using finite domains, which could lead to overly conservative values in the present study.

Flows to deposition holes

Distributions of flows to deposition holes have been presented for the Laxemar base case and for an initial suite of variants for Forsmark. Results for the latter suggest that the distribution of flow to deposition holes is robust with respect to the set of variants considered, and that a given single realization of the discrete-fracture network (DFN) submodel produces representative results. The variants completed thus far do not include alternative conceptual models for the DFN submodel, or variants with respect to its key properties, such as the assumed correlation of size to transmissivity.

The flow distribution to deposition holes is not very sensitive either to the hydrologic properties of the large-scale deformation zones or the time-dependent boundary conditions in a temperate setting. The main controls on this distribution appear to be the DFN submodel, the excavation-damaged zone (EDZ) around tunnels, and spalled zones in the deposition-hole walls (if present).

All model variants presented here are based on freshwater (*i.e.*, uniform density fluid) flow models which likely yield higher groundwater velocities than would be calculated by a model that accounts for density-dependent flow at the coastal interface. This is presumably most important for the mid-temperate case where the coastline is within the model domain, and less important for the late-temperate case where (at Forsmark) the coastline has receded beyond the boundaries of the model domain, or for glacial retreat conditions where high gradients and high flux of fresh water prevail.

Properties of transport paths

Particle-tracking results were produced only for Forsmark variants. A continuous EDZ intersecting all deposition holes and extending along all repository tunnels is included in all Forsmark variants presented here. This is a significant feature for flow and transport, due to the apparent sparseness of the fracture population in the repository volume at Forsmark.

For the Forsmark model variants considered here, the safety-critical lower portion of the distribution of transport resistance F_r is not strongly sensitive to most of the variants that have been modelled. Spalling around deposition holes produces a slight increase in F_r due to increased porosity and wetted surface at the start of each release path. This result is likely sensitive to the assumptions regarding hydraulic properties of the spalled zones, which have been arbitrarily specified for lack of relevant data. Further investigation of the sensitivity of the F_r distribution to assumptions regarding these parameters is warranted.

The lower end of the F_r distribution also shows some sensitivity to stochastic realizations of the DFN submodel. Given that many uncertainties in the DFN submodel have not been resolved, including major conceptual uncertainties (*e.g.* clustering or hierarchical structure), further exploration of these uncertainties is needed. Stochastic variability in the DFN submodel, variability in large-scale deformation zone properties and future climate states can all influence which parts of the repository produce the fastest arrivals, and where these arrive in the biosphere.

None of the model variants in the present study have included large-scale heterogeneity within deformation zones. Models that incorporate large-scale, spatially correlated properties within deformation zones can be expected to exhibit greater large-scale heterogeneity, with more chance for extreme, low F_r pathways, and thus should be considered for further analysis.

7 References

Ahlstrom, S. W., Foote, H. P., Arnett, R. C., Cole, C. R., and Serne, R.J., 1977. Multicomponent mass transport model. Theory and numerical implementation (discrete parcel random walk version), Battelle report BNWL for ERDA, Columbus, Ohio.

Berkowitz, B., Nauman, C., and Smith, L., 1994. Mass transfer at fracture intersections: An evaluation of mixing models. *Water Resources Research*, v. 30, p. 1765-1773.

Brantberger, M., Zetterqvist, A., Anbjerg-Nielsen, Olsson, T., Outters, N., and Syrjänen, P., 2006. Final repository for spent nuclear fuel: Underground design Forsmark, Layout D1. SKB Report R-06-34, Swedish Nuclear Fuel and Waste Management Co., Stockholm.

Follin, S., Stigsson, M., Svensson, U., 2005. Regional hydrogeological simulations for Forsmark - numerical modelling using DarcyTools. Preliminary site description Forsmark area - version 1.2, SKB Report R-05-60, Swedish Nuclear Fuel and Waste Management Co., Stockholm.

Geier, J. E., 1996. Discrete-feature modelling of the Äspö site: 3. Predictions of hydrogeological parameters for performance assessment (SITE-94), SKI Report 96:7, Swedish Nuclear Power Inspectorate, Stockholm.

Geier, J.E., 2005. Groundwater flow and radionuclide transport in fault zones in granitic rock. Ph. D. dissertation, Geosciences Department, Oregon State University, Corvallis, Oregon. Published as SKI Report 05:33, Swedish Nuclear Power Inspectorate, Stockholm.

Geier, J.E., 2008. Discrete Feature Model (DFM) User Documentation. SKI Report 08:xx, Swedish Nuclear Power Inspectorate, Stockholm.

Hartley, L., Hoch, A., Jackson, P., Joyce, S., Mc Carthy, R., Rodwell, W., Swift, B., Marsic, N., 2006a. Groundwater flow and transport modelling during the temperate period for the SR-Can assessman Forsmark area - version 1.2, SKB Report R-06-98, Swedish Nuclear Fuel and Waste Management Co., Stockholm.

Hartley, L., Hoch, A., Jackson, P., Joyce, S., Mc Carthy, R., Swift, B., Gylling, B., Marsic, N., 2006b. Groundwater flow and transport modelling during the temperate period for the SR-Can assessment. Laxemar subarea - version 1.2, SKB Report SKB R-06-99, Swedish Nuclear Fuel and Waste Management Co., Stockholm.

Hartley, L., Hunter, F., Jackson, P., McCarthy, R., Gylling, B., Marsic, N., 2006c. Regional hydrogeological simulations using CONNECTFLOW. Preliminary site description Laxemar subarea - version 1.2, SKB Report R-06-23, Swedish Nuclear Fuel and Waste Management Co., Stockholm.

Hedin, A., 2005. An analytical method for estimating the probability of canister/fracture intersections in a KBS-3 repository. SKB R-05-29, Swedish Nuclear Fuel and Waste Management Co., Stockholm.

Hermanson, J., Forssberg, O., Fox, A., La Pointe, P., 2005. Statistical model of fractures and deformation zones. Preliminary site description, Laxemar subarea, version 1.2, SKB Report R-05-45, Swedish Nuclear Fuel and Waste Management Co., Stockholm.

Janson, T., Magnusson, J., Bergvall, M., Olsson, R., Cuisiat, F., and Skurtveit, E., 2006. Final repository for spent nuclear fuel: Underground design Laxemar, Layout D1. SKB Report R-06-36, Swedish Nuclear Fuel and Waste Management Co., Stockholm.

Munier, R., 2006. Using observations in deposition tunnels to avoid intersections with critical fractures in deposition holes. SKB Report R-06-54, Swedish Nuclear Fuel and Waste Management Co., Stockholm.

Snow, D. T., 1969. Anisotropic permeability of fractured media. *Water Resources Research* 5(6):1273-1289.

SKB, 2004. Deep repository. Underground design premises. Edition D1/1, SKB Report R-04-60, Swedish Nuclear Fuel and Waste Management Co., Stockholm.

SKB, 2005. Preliminary site description: Forsmark area -- version 1.2. SKB Report R-05-18, Swedish Nuclear Fuel and Waste Management Co., Stockholm.

SKB, 2006a. Preliminary site description: Laxemar area -- version 1.2. SKB Report R-06-10, Swedish Nuclear Fuel and Waste Management Co., Stockholm.

SKB, 2006b. Long-term safety for KBS-3 repositories at Forsmark and Laxemar area -- a first evaluation. SKB Technical Report TR-06-09, Swedish Nuclear Fuel and Waste Management Co., Stockholm.

SKB, 2006c. SR-Can Data Report. SKB Technical Report TR-06-25, Swedish Nuclear Fuel and Waste Management Co., Stockholm.

SKB, 2006d. Initial state report for the safety assessment SR-Can, SKB Technical Report TR-06-21, Swedish Nuclear Fuel and Waste Management Co., Stockholm.

Tsang, Y.W., Tsang, C-F., Hale, F.V., and Dverstorp, B., 1996. Tracer transport in a stochastic continuum model of fractured media. Water Resources Research v. 32(10), p. 3077-3092.

Appendix A: Discrete-Feature Modelling Procedures for SR-Can

A digital appendix is available on CD-ROM and can be obtained from SKI. The CD-Rom contains programme codes, files used in the modelling, and results. Moreover, the CD-ROM includes detailed documentation of the procedures that were used to model flow and transport at the Forsmark candidate repository site.

www.ski.se

STATENS KÄRNKRAFTINSPEKTION
Swedish Nuclear Power Inspectorate

POST/POSTAL ADDRESS SE-106 58 Stockholm
BESÖK/OFFICE Klarabergsviadukten 90
TELEFON/TELEPHONE +46 (0)8 698 84 00
TELEFAX +46 (0)8 661 90 86
E-POST/E-MAIL ski@ski.se
WEBBPLATS/WEB SITE www.ski.se